Generation of hiPSC-derived brain microvascular endothelial cells using a combination of directed differentiation and transcriptional reprogramming strategies

Aomeng Cui[1,5], Ronak Patel[2,5], Patrick Bosco[2,5], Ugur Akcan[1], Emily Richters[2], Paula Barrilero Delgado[3], Dritan Agalliu[1,4,6] and Andrew A. Sproul[2,4,6,#]

[1]Department of Neurology, Columbia University Irving Medical Center, New York, NY, USA 10032

[2]Taub Institute for Research on Alzheimer's Disease and the Aging Brain, Columbia University Irving Medical Center, New York, NY, USA 10032

[3]Francisco de Vitoria University, Madrid, Spain

[4]Department of Pathology and Cell Biology, Columbia University Irving Medical Center New York, New York, NY, USA 10032

[5]These first authors contributed equally to the work.

[6]These senior authors jointly supervised the project.

#Lead contact:

Andrew Sproul, Ph.D. E-mail – aas2003@cumc.columbia.edu

Keywords:

blood-brain barrier, NVU, iPSCs, directed differentiation, transcriptional reprogramming, FOXF2, ZIC3, oligomeric Aβ

SUMMARY

The blood-brain barrier (BBB), formed by specialized brain microvascular endothelial cells (BMECs), regulates brain function in health and disease. *In vitro* modeling of the human BBB is limited by the lack of robust hiPSC protocols to generate BMECs. Here, we report generation, transcriptomic and functional characterization of reprogrammed BMECs (rBMECs) by combining hiPSC differentiation into BBB-primed endothelial cells and reprogramming with two BBB transcription factors FOXF2 and ZIC3. rBMECs express a subset of the BBB gene repertoire including tight junctions and transporters, exhibit stronger paracellular barrier properties, lower caveolar-mediated transcytosis, and similar p-Glycoprotein activity compared to primary HBMECs. They can acquire an inflammatory phenotype when treated with oligomeric Aβ42. rBMECs integrate with hiPSC-derived pericytes and astrocytes to form a 3D neurovascular system using the MIMETAS microfluidics platform. This novel 3D system resembles the *in vivo* BBB at structural and functional levels to enable investigation of pathogenic mechanisms of neurological diseases.

INTRODUCTION

The blood-brain barrier (BBB), formed by brain microvascular endothelial cells (BMECs), is critical for the central nervous system (CNS) function. The BBB function is impaired in many neurological disorders but also it imposes a problem for delivery of therapeutics to the CNS[1]. Interactions of BMECs with pericytes and astrocytes via the extracellular matrix (ECM) are critical to assemble the neurovascular unit (NVU), and induce and maintain the BBB properties ranging from: (1) the presence of tight junctions (TJs) which restrict paracellular flux; (2) reduced transcytosis due to the presence of few caveolae; (3) specialized transporters that regulate the passage of nutrients and restrict harmful pathogens; to (4) low expression of leukocyte adhesion molecules (LAMs)[2-6]. Rodent models, although useful for studying mechanisms of CNS diseases, fail to capture patient heterogeneity inherent in multi-factorial neurological

47 disorders and their NVU cells differ from those of humans at the molecular level[7-9]. For example, the
48 mitigating effects of patient comorbidities on traumatic brain injury (TBI) are not captured in rodents;
49 rodent models also do not recapitulate the genetic diversity of Alzheimer's disease (AD) patients[10-12].
50 Additionally, rodents have greater P-glycoprotein drug efflux activity than humans, leading to an
51 underestimation of drug toxicity[9,13]. There is a need to develop *in vitro* human NVU systems with robust
52 BBB properties to model neurological diseases and develop safe, effective therapeutics capable of
53 penetrating the CNS[14-17].
54
55 Primary human BMECs (HBMECs) are scarce, heterogenous, and dedifferentiate in culture[18-20].
56 Human induced pluripotent stem cells (hiPSCs) are a promising alternative due to their reproducibility,
57 scalability, and ability to model various pathological conditions. Over the past decade, several protocols
58 have claimed to generate a homogenous population of "brain" endothelial cells (ECs), termed iPSC-
59 derived BMECs (iBMECs), with high trans-endothelial electrical resistance (TEER) and expression of TJ
60 proteins[21-27]. We recently demonstrated that iBMECs are transcriptomically and functionally analogous
61 to epithelial cells[28]. iBMECs also fail to respond to inflammatory stimuli, limiting their ability to model
62 neuroinflammatory or neurodegenerative diseases[29]. Recent methods have used extended passaging of
63 endothelial progenitor cells (EPCs) to generate ECs (EPC-ECs), with good barrier properties but limited
64 response to inflammatory stimuli[29,30]. Our current understanding of how the human BBB changes in
65 pathological states is limited in part by our ability to generate *bona-fide* brain ECs.
66
67 Comparisons of transcriptome and chromatin accessibility of ECs from various organs have
68 identified several transcription factors (TFs) essential for BMEC identity including FOXF2, FOXQ1,
69 LEF1, and ZIC3[31,32]. FOXF2 is expressed by ECs[31,32] and pericytes[33], and is critical to maintain BBB tight
70 junction integrity and low transcytosis[33]. ZIC3 is upregulated during development, suggesting a potential
71 role in BBB establishment[32,34]. Overexpression of FOXF2 and ZIC3 in primary human umbilical vein

72 endothelial cells (HUVECs) is sufficient to upregulate a limited set of BBB-specific genes[31], so we
73 hypothesized that reprogramming iPSC-derived ECs with FOXF2 and ZIC3 would enable the acquisition
74 of robust BBB properties.
75
76 Here, we describe our novel method to generate iPSC-derived reprogrammed BMECs (rBMECs)
77 by combining an iPSC differentiation step into BBB-primed ECs (bpECs)[35] with FOXF2 and ZIC3-
78 mediated transcriptional reprogramming. rBMECs have higher levels of key BBB transcripts and proteins
79 compared to primary HBMECs and bpECs, exhibit higher TEER, lower transcytosis and equivalent efflux
80 transport compared to HBMECs at the functional level, and respond to angiogenic stimuli. rBMECs
81 respond robustly to oligomerized amyloid-β (oAβ42) by upregulating pro-inflammatory LAMs. Finally,
82 rBMECs cocultured in a 3D microfluidic system with iPSC-derived astrocytes and pericytes form an
83 NVU, demonstrate high TEER levels, and low barrier permeability to tracers, closely resembling the *in*
84 *vivo* human NVU/BBB. Taken together, rBMECs enable faithful *in vitro* modeling of the human BBB for
85 future studies of disease pathogenesis and development of putative clinical therapies.
86
87
88 **RESULTS**
89 **Reprogramming iPSC-derived bpECs into rBMECs**
90 During mammalian embryonic development, the mesodermal layer gives rise to ECs that form the
91 primitive perineural plexus and the CNS vasculature, under the guidance of vascular endothelial growth
92 factor A (VEGF-A) and Wnt/β-catenin signaling (reviewed in[36]). We hypothesized that iPSC-derived
93 rBMECs could be generated using a two-step approach mirroring development (**Figure 1A**). In the first
94 step, iPSCs were differentiated into what we term BBB-primed ECs (bpECs) by sequential exposure first
95 to BMP4/bFGF to generate a mesodermal intermediate followed by VEGF-A/Thymosin β4 using a
96 published protocol with minor modifications[35] (**Figures 1A, S1A**). bpECs were purified from other

97 mesodermal cells by CD31$^+$/VE-cadherin$^+$ expression using fluorescence activated cell sorting (FACS)
98 on day 10 of differentiation (Sort A) and expanded on collagen IV/fibronectin-coated dishes in human
99 endothelial serum-free media supplemented with 1% plasma-derived platelet poor serum, VEGF-A, bFGF
100 and SB431542 (**Figures 1A, B, S1A**). In the second stage, bpECs were transduced with lentiviruses
101 expressing FOXF2 and ZIC3. Transduced and reprogrammed bpECs were grown for 14 days and re-
102 purified by FACS (Sort B) to generate a pure population of rBMECs that could be reliably expanded for
103 five passages after re-purification (**Figures 1A, B, S1A**). By Sort B, bpECs expressed lower levels of
104 CD31 and VE-CADHERIN (CDH5) compared to rBMECs (**Figure 1C**). Sort A efficiency was variable
105 for various iPSC lines ranging from 1.3-5.1% for IMR90 (cl.4), 3.9-7.4% for FA0000010 (FA10), and
106 2.4-3.3% for NCRM5 **(Figure S1C)**; Sort B efficiency was also variable ranging from 56.6-96.1% for
107 IMR90, 83.7-92.3% for FA10, and 34.9-42.6% for NCRM5 (**Figure S1D**).
108
109 **rBMECs express key endothelial and BBB markers and respond to angiogenic stimuli**
110 To characterize rBMECs phenotypically and functionally, we first examined the expression of several
111 EC and BBB proteins. The bpECs and rBMECs derived from all three iPSC lines expressed high levels
112 of key EC identity proteins [e.g. VE-CADHERIN, platelet/endothelial cell adhesion molecule
113 (PECAM1/CD31)] and BBB TJ proteins [CLAUDIN-5, OCCLUDIN, ZONULA OCCLUDENS-1 (ZO-
114 1)] by immunofluorescence (IF) staining (**Figures 1D-F, S1E-J**). The rBMECs had higher CLAUDIN-5
115 (8.1 fold) and OCCLUDIN (1.5 fold) protein levels compared to bpECs by western blot (**Figure 1G-H**).
116 Importantly, rBMECs did not express epithelial cellular adhesion molecule (EPCAM) as assessed by flow
117 cytometry (**Figure S1B)**, indicative of their endothelial identity. We measured the proliferative index of
118 hiPSC-derived ECs by IF staining for Ki67 and DAPI. rBMECs proliferated at a similar rate to bpECs,
119 but at a lower rate than primary HBMECs when cultured without growth factors (VEGF-A and bFGF;
120 **Figure 1I)**. To assess the response to angiogenic stimuli, we performed a wound-scratch assay on EC
121 monolayers (bpECs, rBMECs and HBMECs) treated with either basal media or media supplemented with

122 an angiogenic cocktail [VEGF-A, bFGF, and hepatocyte growth factor (HGF], analyzed the area of wound
123 closure during a 36-hour time lapse as a readout of cell migration and calculated the angiogenic potential
124 (see Methods for details; **Figure 1I-K; S1K-L**). By 36 hours, rBMEC migration increased in response to
125 the angiogenic cocktail compared to control conditions (**Figure 1J**). Primary HBMECs and rBMECs
126 exhibited a comparable angiogenic potential, while bpECs responded more strongly to the angiogenic
127 stimuli (**Figure 1K)**. Overall, these data demonstrate that rBMECs express both key EC and BBB markers
128 and proliferate and migrate in response to angiogenic stimuli.
129

130 **Transcriptome profiling reveals that rBMECs express a subset of the BBB gene repertoire**

131 We used bulk RNA sequencing (bulk RNA-seq) to characterize the CNS EC identity and BBB gene
132 expression in rBMECs. We used principal component analysis (PCA) to compare the rBMEC
133 transcriptome to other human cell types from published datasets[28,37-39]. rBMECs clustered most closely
134 with ECs and furthest apart from choroid plexus cells, epithelial cells, and iBMECs[28] (**Figure 2A; Table**
135 **S1A**). Together with our IF staining and flow cytometry data, this PCA plot confirms that rBMECs have
136 an endothelial identity. The PCA comparison of rBMECs with other EC populations showed that they
137 cluster closer to HBMECs and further away from non-CNS ECs **(Figure 2B; Table S1B).** We performed
138 differential gene expression between rBMECS and HBMECs, or bpECs, to identify which CNS EC and
139 BBB gene signatures are distinct between these populations. A significant number of CNS ECs and BBB
140 genes were distinct between rBMECs and HBMECs (**Figure 2C; Table S1C-D**) or bpECs (**Figure S2B;**
141 **Table S2C, E**), although this difference was higher with HBMECs. Gene ontology (GO) analysis of the
142 differentially expressed genes (DEGs) revealed that pathways related to "blood vessel and vasculature
143 development", "regulation of EC migration" and "BBB permeability maintenance" were upregulated in
144 rBMECs compared to HBMECs **(Figure 2D)**. Several BBB genes encoding for TJs (e.g. CLDN5, OCLN,
145 JAM2), transporters (e.g. SLC2A1, ABCC4, and SLC1A1), receptor-mediated transcytosis (e.g. CAV1,
146 CAV2, LRP10) and ECM components (e.g. COL4A1, COL4A2) were higher in rBMECs compared to

147 HBMECs (**Figure 2E-G**; red); however other BBB genes within these categories were either not
148 significantly different or lower in expression (**Figure 2E-G**; blue). In addition, rBMECs expressed higher
149 levels of CNS EC identity markers (e.g. FOXF2, FOXQ1, SPOCK2, ITM2A, PROM1, LRP8, and
150 APCDD1) compared to primary HBMECs (**Figure 2H; S2A**). Although rBMECs shared a similar gene
151 expression profile with bpECs (**Figure S2B**), several key BBB genes (e.g. ITIM2A, SPOCK2, CLDN5,
152 OCLN, TJP2, SLC2A1 and COL4A1) were upregulated significantly in rBMECs compared to bpECs
153 **(Figure S2C-G)**, suggesting improvement in BBB gene signatures. Moreover, rBMECs showed reduced
154 expression of LAMs (e.g. VCAM1 and SELP) compared to either HBMECs (**Figure 2G),** or bpECs
155 (**Figure S2E**), indicative of a CNS EC identity. In summary, the rBMEC transcriptome analysis shows
156 stronger expression of several CNS EC identity and BBB gene signatures compared to primary HBMECs
157 and bpECs.
158
159 **rBMECs have robust BBB functional properties**
160 We next investigated the functional properties of rBMECs in comparison to bpECs and primary
161 HBMECs. First, we measured TEER over time as a readout of the paracellular EC barrier formed by tight
162 junctions. rBMECs differentiated from the IMR90 line showed a higher average TEER (40.5 ± 4.2 **Ω***cm^2)
163 compared to either bpECs (25.0 ± 0.4 **Ω***cm^2), or primary HBMECs (24.7 ± 3.0 **Ω***cm^2), for >300 hours.
164 The area under the curve (AUC) for the last 100 hours of recording was two-fold higher in rBMECs
165 compared to HBMECs (**Figure 3A, B**). TEER was also increased in rBMECs derived from the other
166 hiPSC lines FA10, NCRM5, and NCRM4 compared to primary HBMECs (**Figure S3A, B, E, F, H, I**).
167 Next, we used three different molecular weight tracers, sodium fluorescein (NaF = 376 Da), 3- and 70-
168 kDa dextran to assess their diffusion (permeability co-efficient) across the EC monolayer in a Transwell
169 system. rBMECs showed a significantly reduced permeability co-efficient (Pe) for the smallest tracer
170 (NaF) across the monolayer compared to bpECs and HBMECs indicative of tighter paracellular barrier
171 **(Figure 3C)**. Although HBMECs showed a significantly higher Pe compared to rBMECs for the medium

172 size tracer (3kDa Dextran), there was no difference between rBMECs and bpECs **(Figure 3D)**. In contrast,
173 the Pe for the 70 kDa Dextran was very low across all three EC lines (rBMECs, bpECs and hBMECs)
174 suggesting very low transcellular transport **(Figure S3C, D).** Overall, the TEER and tracer permeability
175 data demonstrate that rBMECs have a tighter paracellular barrier compared to primary HBMECs and
176 bpECs.
177
178 To assess transcellular rBMEC barrier properties, we examined caveolar-mediated transcytosis by
179 incubating EC monolayers with a fluorescently-tagged bovine serum albumin (BSA; MW = 60 kDa) and
180 measuring its uptake inside cells by flow cytometry. rBMECs and bpECs showed very small changes in
181 the mean fluorescence intensity (MFI) of the intracellular fluorescent BSA compared to HBMECs (**Figure**
182 **3F**), indicative of low caveolae-mediated transcytosis. Finally, we assessed the function of P-
183 GLYCOPROTEIN (PGP, ABCB1), a transporter that effluxes drugs from the brain to the blood[40]. We
184 incubated HBMECs, bpECs, and rBMECs monolayer cultures with Rhodamine 123, which is effluxed by
185 PGP[41], in the presence or absence of a PGP-specific inhibitor, PSC-833. Cells were subsequently analyzed
186 by flow cytometry to assess changes in MFI of the dye. We calculated the efflux rate based on the MFI
187 change in the presence / absence of the inhibitor. HBMECs, bpECs, and rBMECs had comparable efflux
188 rates in response to PSC-833, suggesting similar PGP activity **(Figure 3G, H**). However, rBMECs had a
189 lower fold change in Rhodamine 123 MFI compared to HBMECs **(Figure 3I**) suggesting an overall
190 greater efflux. These data suggest that rBMECs have an increased efflux of rhodamine compared to bpECs
191 and HBMECs, although PGP activity is similar.
192
193 We investigated the ability of rBMECs to respond to pro-inflammatory and disease-relevant stimuli
194 such as oligomeric amyloid-β (1-42) peptides (oAβ42). Most AD patients have amyloid deposits in the
195 cerebral vasculature in post-mortem brains studies[42-44], decreased microvascular density, vBM thickening,
196 BMEC and pericyte damage[45], inflammatory changes in vessels, and microglial activation around blood

197 vessels[46]. We first assessed if oAβ42 affected the paracellular barrier properties of rBMECs. Contrary to
198 published studies[47], there was no change in TEER over 72 hours when rBMECs were exposed to either
199 500 nM or 1 uM oAβ42 (**Figure 3J, K;** data not shown). In contrast, the pro-inflammatory cytokines
200 TNFα and IL1β significantly reduced the rBMEC TEER over 24 hours **(Figure S3J, K),** confirming that
201 rBMECs respond to pro-inflammatory cytokines. To determine if oAβ42 induces EC activation, we
202 extracted mRNA and measured changes in LAMs and chemokines via qPCR. *VCAM-1* was increased by
203 5.2-fold, and *ICAM-1* was increased by 1.7-fold after 24 hours of 1uM oAβ42 exposure (**Figure S3G**).
204 Chemokine ligand 2 (*CCL2*), a major cytokine implicated in the pathogenesis of ischemic stroke[48] and
205 other BBB-compromising pathologies[49,50] and a powerful monocyte and T-cell attractant[48], was also
206 upregulated in rBMECs treated for 24 hours with 1 uM oAβ42 (**Figure S3G**). Therefore, rBMECs respond
207 to 1 uM oAβ42 by upregulating expression of LAMs and pro-inflammatory cytokines. To examine acute
208 effects of oAβ42, we treated rBMECs with 500 nM oAβ42 for 6 hours and analyzed changes in LAMs
209 and pro-inflammatory cytokines by qPCR, western blot, and flow cytometry, as possible downstream
210 effectors of oAβ42-mediated dysfunction. oAβ42 significantly increased mRNA expression of *ICAM-1*
211 and *VCAM-1, E-SELECTIN, CCL2, IL-1β*, *IL-6*, and *TNFα* within 6 hours (**Figure 3L**). Additionally,
212 ICAM-1 and VCAM-1 total and surface protein levels as measured by western blot and flow cytometry,
213 respectively, were upregulated in rBMECs after acute treatment with 500 nM oAβ42 (**Figure 3M-O)**.
214 These data are consistent with recent findings that primary HBMECs upregulate *VCAM-1, ICAM-1, E-*
215 *SELECTIN*, and *CCL2* after treatment with conditioned media from hiPSC-derived cortical neurons
216 harboring the $APP^{Swe/Swe}$ mutation (KM670/671NL)[51]. Finally, we sought to identify potential signaling
217 pathways that might contribute to oAβ42-induced inflammatory phenotypes in rBMECs. Phosphorylation
218 of signal transducer and activator of transcription 3 (STAT3), a key mediator of proinflammatory
219 processes in brain ECs[52,53], was elevated in rBMECs treated with oAβ42 **(Figure S3L-M).** Therefore, β-
220 amyloid peptides act as pro-inflammatory stimuli in rBMECs to upregulate a subset of EC inflammatory
221 gene repertoire that may contribute to increased interactions with immune cells. Overall, these functional

222 studies demonstrate that rBMECs have strong functional BBB properties and are suitable to study immune
223 - EC interactions and the potential impact of disease-relevant stimuli.
224
225 **Modeling the human 3D NVU/BBB using rBMECs and hiPSC-derived astrocytes and pericytes**
226 We next investigated whether rBMECs can interact with iPSC-derived astrocytes and pericytes
227 and generate a fully iPSC-derived human neurovascular unit (NVU) in a 3D microfluidic system (**Figure**
228 **4A**). We generated iPSCs-derived neural crest pericytes (iPCs) following an established protocol, where
229 iPSCs were treated with a neural crest differentiation media supplemented with CHIR99021[54]. iPCs were
230 later sorted on CD146$^+$/PDGFRβ$^+$ to ensure a homogeneous population prior to introduction into the 3D
231 NVU microfluidics system (**Figure S4A**). iPCs expressed PDGFRβ and NG2 (**Figure S4C**) and they had
232 a similar transcriptome profile with primary human pericytes and iPSC-derived neural crest pericytes from
233 prior studies[55] (**Figure S4E**). hiPSCs-derived astrocytes (iACs) were generated from iPSC-derived neural
234 progenitor cells (NPCs) as described[56] with the addition of NFIA transduction of NPCs. iACs expressed
235 high levels of astrocytic proteins GFAP and VIMENTIN (**Figure S4D**) and they were similar at the
236 transcriptome level with primary human astrocytes (**Figure S4F**).
237
238 For the 3D microfluidic system, we used the MIMETAS 64-chip OrganoPlate® comprised of three
239 lanes[57,58]. rBMECs or HBMECs were introduced on Day 0 in the right "blood channel" against a collagen
240 I/IV gel mixture loaded in the middle "ECM" channel, to enable tubule formation. iACs and iPCs were
241 introduced in the left "brain" channel after 2 days and the system was allowed to mature for 10 days with
242 bidirectional flow (**Figure 4A**). By 10 days, rBMECs formed continuous tubules and iACs and iPCs
243 migrated towards the "blood vessel" channel to contact the EC tubules (**Figure 4B)**. rBMEC tubules were
244 positive for the EC markers CD31 and VE-CADHERIN and TJ proteins CLAUDIN-5 and ZO-1 (**Figure**
245 **4C; Movies S1, S2**). In 3D co-cultures of rBMECs with iACs and iPCs, ZO-1$^+$ ECs were in close
246 proximity to S100β$^+$ (astrocyte) and PDGFRβ$^+$ (pericyte) cells, suggesting that iACs and iPCs migrated

247 across the ECM channel to contact the rBMEC tubule (**Figure 4D, E; Movies S3, S4**). Therefore, rBMECs
248 can form tubules and interact with iPSC-derived astrocytes and pericytes to generate a 3D human NVU.
249
250 To assess BBB properties of rBMECs in the 3D microfluidic system, we performed tracer diffusion
251 studies using both small (biocytin, 890Da) and large (dextran, 70kDa) tracers. We introduced the tracers
252 into the blood channel, allowed them to diffuse across the chip for 45 minutes, and measured the mean
253 fluorescent intensity in the middle channel as a readout of tracer leakage through the tubule at three distinct
254 time points (15, 30 and 45 minutes). rBMECs exhibited a significant lower leakage of biocytin and 70kDa
255 dextran compared to primary HBMECs, suggesting that they had tighter paracellular and transcellular
256 barrier properties (**Figure 4F-H**). Moreover, rBMECs cocultured with iACs and iPCs exhibited lower
257 permeability to biocytin compared to rBMECs alone by 45 minutes, suggesting that iPCs/iACs increase
258 the barrier properties of rBMECs (**Figure 4H**). Finally, we measured TEER across the EC tubule in the
259 3D microfluidics system using the OrganoTEER instrument from MIMETAS[57]. While there was
260 considerable variability across experiments, rBMEC tubules displayed on average a six-fold higher TEER
261 compared to HBMEC tubules alone (**Figure 4I, S4G**). rBMEC tubules also had a significantly higher
262 TEER when co-cultured with iACs/iPCs (**Figure 4I, S4G**) consistent with the tracer diffusion studies
263 (**Figure 4H**). Thus, rBMECs form stable and continuous tubules in the MIMETAS 3D microfluidic
264 system, and they interact well with iPCs/iACs to form an iPSC-based NVU with robust BBB properties.
265 This 3D system resembles closely the *in vivo* BBB at both structural and functional levels and can be used
266 to study either NVU - immune dysregulation or the crosstalk between genetic and environmental factors
267 critical for pathogenesis of many neurological diseases.
268
269
270 **DISCUSSION**

271 There generation of an *in vitro* human NVU system with robust BBB properties to model neurological
272 diseases and develop effective therapeutics to enter the CNS has been a major technological hurdle for
273 many decades[14-17]. While several human iPSC-derived BBB models have been developed in the last
274 decade, their utility has been limited by a lack of brain-specific organotypic EC identity and an inability
275 to replicate the multifaceted properties of the BBB. Current methods have either generated ECs with
276 limited BBB properties[30,35], weak immune responses[22,23,26,27,30], generic but not brain-specific cell
277 identity[28,59], or mixed epithelial-endothelial identity[21-24,26,27,60]. In this study, we show that we can generate
278 ECs with robust brain-specific identity and BBB properties (rBMECs) through a combinatorial strategy
279 to initially differentiate hiPSCs into bpECs followed by overexpression of two brain-specific TFs FOXF2
280 and ZIC3 to drive brain organotypicity. rBMECs express higher levels of several key BBB markers
281 belonging to tight junctions, transcytosis, transporters and key CNS EC identity markers at both transcript
282 and protein levels, are capable of undergoing angiogenesis, and respond robustly to oAβ42 treatment (i.e.
283 inflammatory response). In addition, rBMECs have a tighter paracellular barrier, reduced caveolae-
284 mediated transcytosis, and equivalent PGP activity compared to primary HBMECs at a functional level.
285 rBMECs are able to make contacts with iPSC-derived pericytes and astrocytes in a 3D system with flow
286 and strengthen their barrier properties through mutual cell-cell interactions with these other NVU cells,
287 mirroring their 3D organization in the human brain. While several static[61,62] and perfusable[21,24,63,64] iPSC-
288 derived 3D NVU models have been published, our 3D model uses brain-specific ECs that have the
289 capacity to model multiple properties of the human BBB. Overall, our data demonstrate that rBMECs
290 generated through this new approach can be utilized as an *in vitro* human-specific BBB monolayer model
291 and/or a 3D microfluidic NVU model in combination with iPSC-derived PCs/ACs.
292
293 In contrast to our approach of overexpressing FOXF2 and ZIC3 simultaneously, Roudnicky et al.
294 have overexpressed either FOXF2 or ZIC3 alone in ECs generated via a different protocol[59] through
295 adenoviral transduction. FOXF2 overexpression seems to improve some of the BBB properties of ECs by

296 increasing *OCLN* mRNA expression by qRT-PCR, and upregulating Wnt-β-catenin signaling through
297 pathway analysis[65]. FOXF2 also upregulated the inflammatory response pathway. In contrast, ZIC3
298 overexpression had no effect on the barrier properties of ECs[65]. We find that FOXF2 / ZIC3 simultaneous
299 overexpression is sufficient to increase rBMEC barrier properties, but does not induce inflammatory
300 LAMs; *SELP* and *VCAM1* were downregulated, whereas *SELE* and *ICAM1* were unaltered in rBMECs
301 compared to primary HBMECs. Our findings suggest that a FOXF2 / ZIC3 combination is critical for the
302 acquisition of a larger repertoire of BBB properties including barrier strength, suppression of transcytosis
303 genes and suppression of the inflammatory LAMs. However, the precise mechanism by which
304 FOXF2/ZIC3 reprogram bpECs to strengthen BBB characteristics remains unclear. We postulate that
305 bpECs generated via the Praca et al. protocol[35] are more amenable to acquire stronger BBB properties
306 than other EC cell types, as our preliminary efforts to transduce either endothelial progenitor cells[66] or
307 ECs generated from a commercial kit (StemCell Technologies) with FOXF2/ZIC3 failed to generate cells
308 with similar BBB properties as rBMECs. Therefore, FOXF2 and ZIC3 reprogramming seems most
309 effective in a more "plastic" environment present in the BBB-primed EC which already has some BBB-
310 like properties.
311
312 How does Wnt/β-catenin signaling activation affect the BBB repertoire in rBMECs? We have
313 found that administration of CHIR99021, a potent activator the Wnt/β-catenin signaling does not have an
314 additive effect on BBB properties or "brain identity" of rBMECs (data not shown). This was somewhat
315 surprising since a recent study showed that a small molecule cocktail (cARLA) that activates Wnt-β-
316 catenin and cAMP signaling and inhibites TGF-β signaling in generic ECs[67] was sufficient to induce
317 robust BBB properties (tight barrier, high efflux activity) and expression of a subset of brain EC genes[67].
318 However, cARLA failed to increase expression of *FOXF2*, *ZIC3*, and some key BBB genes (e.g. *ITM2A*,
319 *OCLN*) which are robustly upregulated in our rBMECs. cARLA also increased expression of the efflux

320 transporter *ABCB1*, which was not increased by FOXF2 and ZIC3 overexpression, despite comparable
321 levels of PGP efflux activity with primary HBMECs. These two diverse strategies (cARLA vs.
322 FOXF2/ZIC3 reprogramming) can induce complementary BBB properties, whereas FOXF2 and ZIC3
323 reprogramming is critical to upregulate essential "brain identity" markers that cannot be achieved by the
324 small molecule cocktail method. Future studies will determine whether a combination of cARLA and
325 FOXF2/ZIC3 reprogramming strategies can achieve both superior BBB properties and brain
326 organotypicity in ECs.
327
328 Ultimately, one of our goals is to generate an *in vitro* human NVU/BBB model that could faithfully
329 model pathogenic mechanisms of neurological diseases. We investigated the ability of rBMECs to respond
330 to pro-inflammatory and disease-relevant stimuli such as oligomeric amyloid-β (1-42) peptides (oAβ42)
331 elevated in AD patients. In contrast to published studies[68], oAβ42 did not affect barrier tightness of
332 rBMECs, but was sufficient to upregulate significantly expression of pro-inflammatory cytokines and
333 LAMs, including *VCAM-1* and *ICAM-1*. Here, we used a lower, more physiologically relevant dosage of
334 oAβ42 than previously described[68], which is non-toxic in our hands and may explain the lack of effect on
335 the barrier properties. This also suggests that oAβ42, unlike fibrillar forms of Aβ, does not simply damage
336 the BBB to cause dysfunction, but might rather serve as an immune signaling molecule, consistent with
337 the antimicrobial protection hypothesis of AD[69]. Taken altogether, we have established a molecularly and
338 functionally faithful brain EC cell type that can be widely either alone or with other NVU cells to study
339 pathogenic mechanisms of neurological diseases and drug delivery to the CNS.
340
341 **Limitations**: While rBMECs have BBB molecular identity and functional properties, they do not
342 fully recapitulate all aspects of the human BBB. For instance, they do not robustly express the full
343 repertoire of BBB-specific transporters (e.g. MSFD2A). In addition, one major drawback of the
344 differentiation strategy is the low efficiency to produce bpECs (Sort A). Unfortunately, our attempts to

345 reprogram ECs generated from other protocols failed to produce cells with robust BBB properties. Finally,
346 we have not explored the mechanisms by which FOXF2 and ZIC3 drive and sustain BBB properties in
347 rBMECs. This will be a target of future studies.
348
349
350 **ACKNOWLEDGEMENTS**
351 We thank Raphael Lis for providing FOXF2 and ZIC3 expression plasmids, and Paroma Malick in Alex
352 Chavez's lab for subcloning FOXF2 and ZIC3 into pLEX_307. Flow cytometry and cell sorting
353 experiments were performed in the Columbia Stem Cell Initiative Flow Cytometry core facility under the
354 leadership of Michael Kissner. This work was supported by NIH grants from the Heart Lung and Blood
355 Institute [R61/R33 HL159949 and R61/R33 HL159949 (PB)] and National Institute of Aging
356 [RF1AG078352 and RF1AG078352 (PB)]. UA, and DA are also supported by grants from the National
357 Eye Institute (R01EY033994), National Institute of Neurological Disorders and Stroke (R21NS130265),
358 the International OCD Foundation and the Global Lyme Alliance. AAS is also supported by the Henry
359 and Marilyn Taub Foundation and Thompson Family Foundation (TAME-AD).
360
361 **AUTHOR CONTRIBUTIONS**
362 AC, RP, and PB performed experiments, analyzed data, and drafted the manuscript. UA performed the
363 bioinformatic analysis. ER performed some experiments and provided invaluable technical support. PBD
364 performed experiments and analyzed data. AAS and DA conceptualized the project, provided the funding,
365 oversaw all work, and drafted the manuscript. All authors edited the manuscript.
366
367 **DECLARATION OF INTERESTS**
368 The authors declare no competing interests.
369

370 **STAR* METHODS**

371 **KEY RESOURCE TABLE**

REAGENT or RESOURCE	SOURCE	IDENTIFIER
Antibodies		
Goat polyclonal PDGFRβ Antibody	R&D	Cat#AF385; RRID: AB_355339
Rabbit monoclonal anti-Vimentin antibody	Cell Signaling Technology	Cat#D21H3; RRID: AB_10695459
Mouse monoclonal Neural/Glial Antigen 2 (NG2) Antibody (9.2.27), eBioscience™	Thermo Fisher	Cat#14-6504-82; RRID: AB_10870987
Mouse monoclonal α-Smooth Muscle antibody	Sigma Aldrich	Cat#A5228; RRID: AB_262054
Mouse monoclonal Anti-Human CD31 antibody (Clone JC70A)	Agilent	Cat#M082301-2; RRID: AB_2114471
Rabbit polyclonal VE-Cadherin antibody	Abcam	Cat#ab33168; RRID: AB_870662
Rabbit polyclonal anti-GAPDH antibody	Sigma	Cat#G9545; RRID: AB_796208
Mouse monoclonal anti-S100β	Sigma-Aldrich	Cat#S2532; RRID: AB_477499
Rabbit monoclonal anti-VCAM-1	Abcam	Cat#ab134047; RRID: AB_2721053
Rabbit monoclonal anti-ICAM-1	Cell Signaling	Cat#67836T; RRID: AB_2799738
Mouse monoclonal anti-GFAP	EMD Millipore	Cat#MAB360; RRID: AB_11212597
Rat Monoclonal anti-Ki-67 Antibody (SolA15)	Thermo Fisher	Cat#14-5698-82; RRID: AB_10854564
Mouse monoclonal anti-Claudin-5	Thermo Fisher	Cat#35-250-0; RRID: AB_2533200
Rabbit polyclonal anti-ZO-1	Thermo Fisher	Cat#61-7300; RRID: AB_2533938
Rabbit polyclonal anti-GLUT-1	Thermo Fisher	Cat#PA5-16793; RRID: AB_10986893
Mouse monoclonal anti-Occludin	Thermo Fisher	Cat#33-1500; RRID: AB_2533101
Mouse PhosphoPair STAT3 (Tyr705) Antibody Set	Biolegend	Cat.# 699952; RRIDs: AB_2861053, AB_10897947

Mouse monoclonal anti-EpCAM Direct Conjugated Antibody, Alexa Fluor 488	BioLegend	Cat#324210; RRID: AB_756084
Mouse monoclonal anti-PECAM-1 Direct Conjugated Antibody, APC	BioLegend	Cat#303116; RRID: AB_1877151
Recombinant human monoclonal anti-VE-Cadherin Direct Conjugated antibody, APC	Miltenyi Biotech	Cat#130-125-985; RRID: AB_2655162
Mouse monoclonal anti-VE-Cadherin Direct Conjugated Antibody, PE	BioLegend	Cat#348506; RRID: AB_2077978
Mouse monoclonal anti-ICAM-1 Direct Conjugated Antibody, FITC	BioLegend	Cat#353107; RRID: AB_10898317
Mouse monoclonal anti-VCAM-1 Direct Conjugated Antibody, APC	Biolegend	Cat#305809; RRID: AB_2304307
Mouse monoclonal anti-CD184 Direct Conjugated Antibody, APC	BioLegend	Cat#306509; RRID: AB_314615
Mouse monoclonal anti-CD133 Direct Conjugated Antibody, PE	BioLegend	Cat#372803; RRID: AB_2632879
Mouse monoclonal anti-CD271 Direct Conjugated Antibody, FITC	BioLegend	Cat#345103; RRID: AB_1937226
PE anti-human CD140b (PDGFRβ) Antibody	BioLegend	Cat#323605; RRID: AB_2299493
PE/Cyanine7 anti-human CD146 Antibody	BioLegend	Cat#361008; RRID: AB_2562983
Goat anti-mouse IgG (H+L), HRP conjugate	Thermo Fisher	Cat#31430; RRID: AB_228307
Goat anti-rabbit IgG (H+L), HRP conjugate	Thermo Fisher	Cat#31466; RRID: AB_10960844
Donkey anti-mouse IgG (H+L) Secondary Antibody, Alexa Fluor 488	Thermo Fisher	Cat#A21202; RRID: AB_141607
Donkey anti-mouse IgG (H+L) Secondary Antibody, Alexa Fluor 568	Thermo Fisher	Cat#A10037; RRID: AB_2534013

Donkey anti-rabbit IgG (H+L) Secondary Antibody, Alexa Fluor 568	Thermo Fisher	Cat#A10042; RRID: AB_2534017
Goat anti-rabbit IgG (H+L) Secondary Antibody, Alexa Fluor 647	Thermo Fisher	Cat#A21245; RRID: AB_2535813
Chemicals, Peptides, and Recombinant Proteins		
Recombinant human FGF-2	R&D Systems	Cat#3718-FB
Recombinant human VEGF-165	R&D Systems	Cat#293-VE-050/CF
Recombinant human VEGF-165	Stem Cells Tech.	Cat#78073.1
Recombinant human bFGF	Peprotech	Cat#100-18C-100ug
Recombinant human HGF	Peprotech	Cat#100-39H
Recombinant human Thymosinβ4	R&D Systems	Cat#3390/100U
Recombinant human BMP-4	R&D Systems	Cat#314-BP-500/CF
Recombinant β-amyloid (1-42)	rPeptide	Cat#A-1163-2
Recombinant human TNFα	R&D Systems	210-TA-020/CF
Recombinant human IL-1β	R&D Systems	201-LB-005/CF
Human transferrin	Sigma-Aldrich	Cat#T3309
Sodium fluorescein	Sigma-Aldrich	Cat#46960-25G-F
Dextran, 3 kDa, Alexa Fluor 680	Thermo Fisher	Cat#D34681
Dextran, 70 kDa, CF770	Biotium	Cat#80123
Collagen from human placenta, type IV	Sigma-Aldrich	Cat#C5533
Fibronectin from human plasma	Sigma-Aldrich	Cat#F2006
Cultrex Stem Cell Qualified RGF Basement Membrane	R&D	Cat#3434-010-02
Insulin solution	Sigma-Aldrich	Cat#19278
Puromycin	Sigma-Aldrich	Cat#P8833
Poly-D-Lysine	MP Biomedicals	Cat#0215017510
SB 431542	Selleck Chemicals	Cat#S1067
CHIR 99021	Tocris	Cat #4423

Collagenase Type IV	StemCell Technologies	Cat#07909
Plasma derived-platelet poor serum	Sigma-Aldrich	Cat#P2918
Knockout serum replacement	Thermo Fisher	Cat#10828028
Fetal Bovine Serum, heat-inactivated	Sigma Aldrich	Cat#12306C
Bovine serum albumin	Sigma-Aldrich	Cat#A9576
Bovine serum albumin	Sigma-Aldrich	Cat#A9418
Accutase	Thermo Fisher	Cat#A11105-01
ReleSR	StemCell Technologies	Cat#100-0483
Trypsin-EDTA (0.05%)	Thermo Fisher	Cat#25300-054
β-mercaptoethanol	Thermo Fisher	Cat#21985-023
GlutaMAX	Thermo Fisher	Cat#35050-061
MEM non-essential amino acids	Thermo Fisher	Cat#11140-050
Penicillin-streptomycin (10,000 U/mL)	Thermo Fisher	Cat#15140-122
B-27 Supplement, minus vitamin A	Gibco	Cat#12-587-010
N-2 Supplement	Gibco	Cat#17502048
Rhodamine 123, FluoroPure™ grade	Invitrogen	Cat#R22420
Albumin from Bovine Serum (BSA), Alexa Fluor™ 594 conjugate	Invitrogen	Cat#A13101
PSC-833	Tocris	Cat#4042
SuperBlock Blocking Buffer in PBS	Thermo Fisher	Cat#37515
Triton-X	Thermo Fisher	Cat#A16046
Tween 20	Thermo Fisher	Cat#BP337
SuperBlock T20 Blocking Buffer	Thermo Fisher	Cat#37536
CF® Dye Biocytin CF640	Biotium	Cat#92007
CellTag 700 Stain	LI-COR	Cat#926-41090
eBioscience Fixable Viability Dye eFluor 780	Thermo Fisher	Cat#65-0865-14
Critical commercial assays		
BCA Protein Assay Kit	Millipore Sigma	Cat#71285-3

SuperSignal West Pico PLUS Chemiluminescent Substrate	Thermo Fisher	Cat#34577
RNeasy Mini Kit	Qiagen	Cat#74104
RNeasy Micro Kit	Qiagen	Cat#74004
Maxima First Strand cDNA Synthesis Kit for RT-qPCR	Thermo Fisher	Cat#K1642
Lipofectamine 3000 Transfection Kit	Thermo Fisher	Cat#L3000001
12mm diameter, 12µm pore transwell insert	Corning	Cat#3401
Human endothelial serum-free media	Gibco	Cat#11111044
Endothelial Cell Growth Medium MV2	PromoCell	Cat#C-22121
Astrocyte Medium Kit	ScienCell	Cat#1801
Pericyte Medium Kit	ScienCell	Cat#1201
F-12, phenol red free	R&D	Cat#M25350
DMEM / F12 (1:1)	Gibco	Cat#11320-033
F12	Gibco	Cat#11765-054
IMDM	Gibco	Cat#12440-053
DMEM	Gibco	Cat#11965-092
Knockout DMEM	Gibco	Cat#10829-018
Experimental Models: Cell lines		
HEK293T	ATCC	Cat#CRL-1573
Irradiated CF1 mouse embryonic fibroblasts	Thermo Fisher	Cat#A34181
Primary Human Umbilical Vein Endothelial Cells	ATCC	Cat#PCS-100-010
Primary Human Brain Microvascular Cells	Cell System	Cat#ACBRI376
Human Brain Vascular Pericytes	ScienCell	Cat#1200
Human Astrocytes	ScienCell	Cat#1800
iPS(IMR90)-4	WiCell	RUID# WISCi004-B
FA0000010 (FA10)	RUCDR	RUID# CUIMCi001-A

ND50025 (NCRM-4)	RUCDR/NINDS Collection	RUID# CR0000004, Clone ID: R149482761
ND50031 (NCRM-5)	RUCDR/NINDS Collection	RUID#CR0000005, Clone ID: R149506778
Oligonucleotides		
Primers for RT-qPCR: listed in Supplementary Table A		
Recombinant DNA		
FOXF2 lentiviral construct	This manuscript	Backbone: Addgene_41392
ZIC3 lentiviral construct	This manuscript	Backbone: Addgene_41392
NFIA lentiviral construct	Addgene	Backbone: Addgene_141403
Software and Algorithms		
ImageJ	NIH	https://imagej.nih.gov/ij/
FlowJo	FLOWJO LLC	https://www.flowjo.com/
GraphPad Prism 9.0.0	GraphPad Software Inc.	https://www.graphpad.com/features
R studio v2023.12.0+369	R Studio	R Studio
EdgeR package 2.1	BioConductor	https://github.com/alexdobin/STAR
STAR Alligner v2.5.2a	Dobin et al. 2013. STAR: ultrafast universal RNA-seq aligner. Bioinformatics 29(1):15-21.	
FastQC	Babraham Institute	http://www.bioinformatics.babraham.ac.uk/projects/fastqc/
subread	https://academic.oup.com/nar/article/41	https://subread.sourceforge.net/

	/10/e108/1075719?login=false	
Zen 3.9	Zeiss Company	https://www.zeiss.com/microscopy/en/products/software/zeiss-zen.html

372

373 **Resource availability**

374 For further information and requests for resources, reagents, or code, please contact corresponding authors
375 Andrew Sproul (aas2003@cumc.columbia.edu) and Dritan Agalliu (da191@cumc.columbia.edu).

376

377 **Materials availability**

378 Plasmids from this study are available upon reasonable request. Please refer to STAR*Methods section
379 for resources.

380

381 **Experimental Models**

382 **Human iPSC line maintenance:** For all primary experiments, human control iPSC line IMR90-cl.4 was
383 used (WiCell)[70]. For additional experiments, human control iPSC line FA0000010 (FA10), ND50031
384 (NCRM-5), and ND50025 (NCRM-4) were used (RUCDR). IMR90-cl.4 and NCRM-4 were derived from
385 female donors, while FA10 and NCRM-5 were from male donors. For differentiation into bpECs or NPCs,
386 iPSCs were maintained on feeder culture of irradiated CF1 mouse embryonic fibroblasts (MEFs) with
387 Human Embryonic Stem cell Medium (HUESM): knockout DMEM, 20% knockout serum replacement
388 (Thermo Fisher), 2mM Glutamax (Thermo Fisher), 0.1 mM MEM non-essential amino acids (Thermo
389 Fisher), 1% penicillin-streptomycin (Thermo Fisher), and 0.1 mM β-mercaptoethanol (Thermo Fisher)
390 supplemented with 20 ng/mL bFGF (R&D) and passaged when 80-90% confluent. Feeder-free hiPSCs
391 were maintained in StemFlex medium (Thermo Fisher) containing penicillin-streptomycin (Thermo
392 Fisher) on Cultrex-coated plates (Bio-Techne). Cultures were passaged using ReLeSR (StemCell
393 Technologies) every 3-4 days.

394

395 **Directed differentiation of hiPSCs into BBB-primed endothelial cells (bpECs):** hiPSCs were
396 differentiated into bpECs (our term) as previously reported with slight modifications[35]. hiPSCs were
397 dissociated with collagenase-IV, and cell aggregates were plated in chemically defined media (CDM):
398 50% IMDM (Thermo Fisher), 50% Ham's F12 (Thermo Fisher), 5 mg/mL bovine serum albumin (Thermo
399 Fisher), 15 ug/mL transferrin (Sigma-Aldrich), 0.1 mM β-mercaptoethanol (Thermo Fisher), 7 ug/mL
400 insulin (Sigma-Aldrich), 1% penicillin-streptomycin (Thermo Fisher) on 1 ug/mL fibronectin (Sigma-
401 Aldrich) coated 10 cm dishes from one well of a 6-well plate to one 10 cm dish. CDM was supplemented
402 with 10 ng/mL BMP4 (R&D) for 1.5 days to induce mesodermal differentiation and 50 ng/mL BMP4 and
403 20 ng/mL bFGF (R&D) for the next 3.5 days for further expansion of mesodermal lineage cells. From
404 days 5 to 10, endothelial differentiation was initiated by supplementing CDM media with 50 ng/mL VEGF
405 (R&D) and 100 ng/mL thymosin-β4. Endothelial cells were purified at day 10-11 by FACS for
406 $CD31^+/CDH5^+$ cells. These endothelial cells, now termed bpECs, were plated on collagen IV/fibronectin
407 coated plates at a density of 30,000 to 35,000 cells/cm^2 and fed EC medium (Human Endothelial Serum
408 Free Medium (Thermo Fisher) supplemented with 1% human serum (Sigma-Aldrich) supplemented with
409 50 ng/mL VEGF165 (R&D), 20 ng/mL bFGF (R&D), and 10 μM SB431542 (Sigma-Aldrich). bpECs
410 were expanded and passaged 1:2 to 1:3 every 7-10 days and generally used for five passages.

411

412 **Reprogramming of bpECs into rBMECs**: bpECs were plated at 30,000-35,000 cells/cm^2 on collagen
413 IV/fibronectin coated plates using EC media supplemented with 50 ng/mL VEGF165, 20 ng/mL bFGF
414 and 10 uM SB431542. On day 2, bpECs were transduced with FOXF2 (~$1x10^6$ lentiviral p24 units/mL of
415 medium) and ZIC3 (~$7.5x10^5$ lentiviral p24 units/mL of medium) as determined by Lenti-X GoStix
416 (Takara). Successfully infected cells were selected with 1 ug/mL puromycin (Sigma) for 24 to 48 hours.
417 Infected bpECs were purified via FACS for $CD31^+$/VE-cadherin$^+$ cells on day 14. FACS-purified and
418 infected bpECs, referred to as rBMECs, were plated on collagen IV/fibronectin coated plates 25,000-

419 35,000 cells/cm^2 and expanded until confluent. rBMECs were passaged at high density using 1:2 splits
420 every 7-10 days and used within five passages.
421
422 **Generation of lentiviral vectors and lentiviruses**: FOXF2 and ZIC3 were subcloned into pLex_307,
423 which was a gift from David Root (Addgene), and verified by Sanger sequencing (Azenta). FUW-tetO-
424 NFIA was a gift from Lorenz Studer (Addgene)[71]. FUdeltaGW-rtTA was a gift from Konrad Hochedlinger
425 (Addgene)[72]. psPAX2 was a gift from Didier Trono (Addgene). VSV.G was a gift from Tannishtha Reya
426 (Addgene)[73]. Lentiviral particles for FOXF2, ZIC3, NFIA, and rtTA were generated in HEK293 as
427 described previously[74], using the psPAX2/VSV.G 2nd generation system. Efficacy of lentiviral particles
428 was confirmed by infection and subsequent qPCR.
429
430 **Fluorescence-activated cell sorting (FACS):** Cells were dissociated into single cell suspension using
431 Accutase (ThermoFisher) and washed with base medium (CDM for EC differentiation at day 10 and EC
432 media for rBMECs). Cell suspensions were incubated with FACS buffer (10% KOSR in DPBS) with
433 fluorescently tagged antibodies (CD31-FITC, VE-cadherin-APC) for 30 min at room temperature
434 protected from light. Cell suspensions were washed with FACS buffer and cell pellets were resuspended
435 for FACS by filtering through 0.45 μM filters (Fisher Scientific) to remove cell aggregates. bpECs or
436 rBMECs were sorted on the Sony MA900 cell sorter and double positive CD31$^+$/VE-cadherin$^+$ cells were
437 subsequently expanded.
438
439 **Primary endothelial cell, pericyte, and astrocyte cultures**: HBMECs (Cell Systems) were cultured in
440 Endothelial Cell Growth Medium MV 2 (Promocell). PCs were cultured in Pericyte Media (PM,
441 ScienCell), and ACs were cultured in Astrocyte Media (AM, ScienCell). HBMECs and PCs were plated
442 onto collagen IV and fibronectin coated plates, while ACs were plated onto either Matrigel or Cultrex-

443 coated plates. All cells were supplemented with media every other day and passaged using Accutase once
444 90% confluent.
445
446 **Generation of iPSC-derived pericytes:** Briefly, feeder-free iPSCs were differentiated into neural crest
447 pericytes following an established protocol, where iPSCs were treated with a neural crest differentiation
448 media supplemented with CHIR99021 and subsequently treated with Pericyte Media (ScienCell)[54]. Cells
449 were later sorted on CD146+/PDGFRβ+ to ensure a homogeneous population prior to introduction into
450 the BBB triculture system.
451
452 **Generation of iPSC-derived astrocytes:** hiPSCs were differentiated into a neural progenitor cells
453 (NPCs) using dual-SMAD inhibition in embryoid bodies as previously described[56]. On day -1, NPCs were
454 dissociated using Accutase and plated at a density of 15,000 cells/cm^2 in N2/B27 media on Cultrex-coated
455 plates. On day 0, the media was replaced with supplemented Astrocyte Media (2% fetal bovine serum,
456 and proprietary astrocyte growth factor supplement) (ScienCell). On day 1, differentiating cells were
457 transfected with lentiviral particles carrying dox-inducible NFIA and rtTA (Addgene). Cells were fed
458 every other day using astrocyte media supplemented with doxycycline (2µg/mL) (Sigma-Aldrich). Cells
459 were split at 90-95% confluence roughly once every seven days and re-plated at a density of 15,000
460 cells/cm^2 for 30 days. At this stage, astrocytes were split 1:3 once 90-95% confluent and were expanded,
461 banked, and utilized.
462
463 **RNA isolation and RT-qPCR:** RNA was extracted using the RNeasy Plus Micro Kit (Qiagen) and
464 resuspended in 30 µl of RNAse-free water. RNA quantity and quality were assessed with a Nanodrop One
465 (ThermoScientific). For qPCR, 100-250 ng of RNA was transcribed into cDNA using the Maxima First
466 Strand cDNA Synthesis Kit (Thermo Fisher). Gene expression was assessed using the FAST SYBR Green
467 Master Mix (ThermoFisher Scientific) with primer sets (Integrated DNA Technologies) for target genes

468 on a QuantStudio 7 Flex system (Applied Biosystems) and CFX Opus 384 (Bio-Rad). Gene expression
469 for target genes were normalized to GAPDH and fold changes were calculated as $\Delta\Delta C_t$.
470
471 **Western blotting**: Endothelial cells were harvested using RIPA Lysis Buffer supplemented with Halt
472 protease and phosphatase inhibitors single-use cocktails (Thermo Fisher) on ice. 10 μg of lysates and 1x
473 Laemmli sample buffer/5% β-mercaptoethanol were boiled at 95° C for 5 min. SDS-PAGE was performed
474 by loading samples on Bolt 4–12% gradient Bis-Tris gels using Bolt MOPS buffer (Thermo Fisher).
475 Nitrocellulose membranes were first blocked with Superblock TBS buffer/0.1% Tween 20 Thermo Fisher)
476 for 1h, and then incubated overnight at 4° C with the following primary antibodies diluted in
477 Superblock/0.1% Tween 20: Claudin-5 (1:1000; Thermo Fisher), Occludin (1:1000; Thermo Fisher),
478 VCAM-1 (1:1000, Abcam), pSTAT3 (1:1000, BioLegend), STAT3 (1:1000, BioLegend) and GAPDH
479 (1:5000; Thermo Fisher). After 3 washes with TBS/0.1% Tween-20, membranes were then incubated with
480 the appropriate HRP-conjugated secondary antibody (1:5000, Thermo Fisher) for 1 hour, and washed 3
481 more times with TBS/0.1% Tween-20. Pierce ECL western blotting substrate or SuperSignal West Pico
482 PLUS chemiluminescent substrate (Thermo Fisher) were used to develop chemiluminescence and blots
483 were imaged using the Bio-Rad Chemidoc MP system.
484
485 **Transendothelial electrical resistance (TEER) measurement:** TEER measurements were carried out
486 using the ECIS Z-theta instrument on the 96W20idf array at 4000 Hz frequency. Briefly, 20,000 cells
487 were plated on poly-D-lysine and collagen IV/fibronectin-coated 96-well electrode array plates in the
488 respective medium for each cell type. Resistance was recorded for 250-300 hours and medium was
489 changed every other day. The resistance curve was generated using PRISM (GraphPad) and the area under
490 the curve (AUC) was measured either for last 100 hours of recording or for the duration of oAβ42 or
491 cytokine treatment (72hr or 24hr) from 6-8 wells using the AUC PRISM function.
492

493 **Tracer permeability assay:** Tracer permeability assay for determination of paracellular permeability was
494 performed as previously described[75]. rBMECs, bpECs and hBMECs were cultured on 12-well
495 polycarbonate Transwell inserts (0.4 uM, Corning) for 10 days to ensure a complete monolayer. Growth
496 factors were removed for 24 hours prior to assay. A full media change was performed on bottom chamber
497 (1.5 mL) and all 3 tracers (NaF- 10 ug/mL, 3 kDa dextran - 25 ug/mL and 70 kDa dextran- 25 ug/mL)
498 were added on top chamber in 0.5 mL medium to start the assay. As soon as tracers were added, 100 uL
499 medium was collected from bottom chamber as 0 min collection and replaced with 100 uL fresh media
500 for each well, followed by serial collection for every 10 min for up to 60 min. Fluorescent intensities were
501 measured and clearance slopes were calculated using:
502

503 $$\Delta V = C_{bottom} \times V_{bottom} / C_{upper},$$

504 C_{bottom} and C_{upper} are fluorescent intensities measured for each tracer in top and bottom chamber
505 respectively, V_{bottom} is volume of media in bottom chamber (1.5 mL)
506

507 $$P_{filter} = PS_{filter}/s \quad \text{and} \quad P_{cell+filter} = PS_{cell+filter}/s,$$

508 P_{filter} and $P_{cell+filter}$ are permeability coefficient for blank insert and insert with cells, PS_{filter} and $PS_{cell+filter}$
509 are which can be obtained by regression plot of ΔV against time for blank insert and insert with cells.
510

511 $$1/P_e = 1/ P_{cell+filter} - P_{filter},$$

512 Pe is permeability co-efficient for endothelial cell monolayer
513

514 **Wound scratch assay:** Cells were plated at a density of 100K/well (24-well plate). Once confluent, cells
515 were fed their standard media absent VEGF and bFGF supplementation. Monolayers were scratched in
516 the center of each well using the Autoscratch automated scratch machine (BioTek). Wells were then
517 treated with either control media, 100 ng/mL VEGF, or an angiogenic cocktail consisting of VEGF (37.5

518 ng/ml), bFGF (37.5 ng/ml), and HGF (37.5 ng/ml). Plates were cultured and imaged automatically every
519 6 hours using the Cytation5 plate reader (BioTek) and software, for HBMECs (24 hrs) and bpECs and
520 rBMECs (36 hrs) during culture in a BioSpa incubator (BioTek). Each well was quantified for % surface
521 area of the wound utilizing an ImageJ plug-in for identifying the area of the scratch[76], which was then
522 normalized to the original size of the wound for each well. To compare cell types, we calculated an
523 angiogenic potential, where:
524

525 $$\text{angiogenic potential} = \int \text{untreated wound area} - \int \text{wound area with angiogenic cocktail}$$

526

527 **Ki67 quantification assay**: After the wound scratch assay was performed, cells were fixed with 4% PFA.
528 Cells were blocked as described above and stained with Ki67 antibody (1:500). Cells were labeled with a
529 GFP secondary antibody and DAPI. Wells were imaged for DAPI and GFP fluorescence on the BioSpa
530 as done previously. Each well was quantified for proliferative index, where:
531

532 $$\text{Proliferative Index} = \frac{\text{Number of Ki67+ cells}}{\text{Number of DAPI+ cells}}$$

533

534 Cells were identified as Ki67 or DAPI positive using the annotation machine learning tool from the QuPath
535 software[77].
536

537 **Uptake and transporter assays**: As previously described[60], cells were plated at a density of 100K/well
538 (24-well plate) and subcultured until confluent. First, cells incubated with either 1 mg/mL unlabeled BSA
539 or 1 mg/mL BSA-Alexa 594 for 1 hour at 37º C. Cells were then dissociated into single cell suspension,
540 stained for eFluor 780, fixed with 4% PFA, and analyzed for Alexa594 median fluorescence intensity
541 (MFI). For the transporter assay, cells were incubated with Rhodamine 123 (10 uM) for 1 hr at 37º C. To

542 assess the effect of P-glycoprotein (Pgp) efflux, cells were pretreated with PSC-833 (a specific Pgp
543 inhibitor) for 1 hr prior to Rhodamine treatment. Cells were dissociated into single cell suspension, stained
544 for eFluor 780, fixed with 4% PFA, and analyzed for Rhodamine MFI. NPCs were utilized as a positive
545 control due to their low level of Pgp efflux. Data were normalized to the unstained MFI for each cell type,
546 which we termed fold change in MFI. To calculate Pgp efflux, we calculated the percent change in MFI
547 with and without PSC-833:
548

549 $$\text{PGP efflux} = \frac{\text{MFI}_{\text{PSC}-833} - \text{MFI}_{\text{Rhodamine}}}{\text{MFI}_{\text{Rhodamine}}}$$

550

551 **Amyloid-β42 oligomerization and treatment:** Amyloid-β42 was monomerized, stored and later
552 oligomerized as previously described[78,79]. In brief, Aβ(1-42) (rPeptide, 1 mg) vial was allowed to
553 equilibrate to room temperature. Peptides were resupended in ice-cold hexafluoroisopropanol (Sigma-
554 Aldrich) to achieve 1 mM concentration directly in a vacuum-sealed vial using a Hamilton syringe. The
555 suspension was divided into 8 equal aliquots by volume using a Hamilton syringe into low protein binding
556 Eppendorf tubes, incubated at room temperature for 2 hours and dried on speedvac at 800g for 25ºC. Upon
557 drying monomerized Aβ(1-42) films can be stored at -80ºC in sealed tubes. For generating oligomers,
558 Eppendorf tubes containing Aβ(1-42) peptide films were equilibrated to room temperature, resuspended
559 in DMSO to achieve 5 mM concentration and sonicated at 17ºC for 10 min for complete resuspension.
560 Oligomerization was induced by adding phenol-red free F12 to achieve final concentration of 100 uM and
561 incubated at 4ºC for 24 to 48 hours. rBMEC monolayers were treated with oAβ at 500 nM or 1 uM
562 concentrations for the indicted period of time and F12 was used a vehicle control.
563

564 **3D microfluidic BBB culture model:** OrganoPlate 3-lane-64 plates (MIMETAS) were used to generate
565 a 3D microfluidic system of the BBB. In each chip, the center channel was filled with an ECM gel, an

566 endothelial tubule was generated in the right channel, and a mixture of iPSC-derived astrocytes and
567 pericytes was seeded in the left channel and allowed to migrate towards the endothelial cells during culture
568 upon a bidirectional OrganoFlow rocker (MIMETAS).
569
570 *ECM generation and endothelial channel coating:* On day -1, the center ECM channel was filled with a
571 4:1 ratio of collagen I (5 mg/ml) and collagen IV solution (5 mg/mL), incubated at 37º C for 15 min, and
572 covered with PBS to prevent collagen gel from drying. The right channel inlet was coated using fibronectin
573 (10 ug/mL) and collagen IV (10 ug/mL) overnight.
574
575 *Endothelial cell seeding*: On day 0, endothelial cells were singularized and resuspended to achieve a
576 15,000 cells/uL concentration. Cells were seeded in the right channel outlet at a density of 30,000
577 cells/chip. Plate was placed on a 75º plate stand from the manufacturer and incubated at 37º C for four to
578 five hours to allow endothelial cells to settle against the gel. Then, outlets were replenished with
579 endothelial media and the plate was placed on the OrganoFlow rocker to alternate between -7 to +7º every
580 8 minutes. After a day or two, endothelial cells formed an open tubule in the right channel.
581
582 *Astrocyte and pericyte channel coating and cell seeding:* On day 1, the left channel inlet was coated with
583 Matrigel. Primary astrocytes (ACs) and iPSC-derived ACs were singularized and resuspended in AM-PM
584 media (2:1 ratio of AM:PM) to achieve a 15,000 cells/uL concentration. Primary pericytes (PCs) and
585 iPSC-derived iPCs were similarly singularized and resuspended in AM-PM to achieve a 7,500 cells/uL
586 concentration. Primary astrocytes and primary pericytes were mixed at a ratio of 1:1 and seeded in the left
587 channel outlet for each chip to achieve 15,000 ACs and 7,500 PCs per chip. The plate was rested on the
588 stand for four to five hours at 37º C to allow pericytes and astrocytes to settle against the gel. Finally,
589 outlets were replenished with AM-PM and the plate was placed back on the OrganoFlow rocker for

590 continuous culture until Day 10. Media was replenished every other day. Beginning on day 6, chips were
591 replenished with their standard EC media without bFGF and VEGF supplementation.
592
593 **Tracer permeability assay**: On day 10 post seeding, a 70-kDa dextran (0.5 ug/mL) and Biocytin tracer
594 (0.5 ug/mL) were introduced into the right inlet and outlet wells (40 uL and 30 uL, respectively). The gel
595 inlet, left inlet, and left outlet wells were filled with 20 uL media without tracer. Then, the plate was placed
596 onto the OrganoFlow rocker and imaged every 15 minutes in the LI-COR. The fluorescence intensity for
597 each well was quantified with the Odyssey SA system. Analysis was performed as the normalized
598 fluorescence intensity over the ECM channel center well, which represented the leakage from the right
599 vascular channel into the left brain channel:
600

601 $$\text{Normalized Intensity} = \frac{\text{Middle ECM channel intensity}_{\text{sample}}}{\text{Mean middle channel intensity}_{\text{ECM}}}$$

602
603 where ECM chips only had a control gel, representing the leakage without cells present. Samples were
604 analyzed using a two-way ANOVA test.
605
606 **3D TEER assay**: Chips were assayed for TEER on day 10 post seeding. After the plate was introduced
607 into the OrganoTEER device, TEER values were measured for the vascular channel using the "low TEER"
608 setting, which is suitable for endothelial cells, per the manufacturer. Measurements for each condition
609 were compared using a one-way ANOVA test.
610
611 **Immunofluorescence and microscopy**
612 *Staining of monolayer endothelial cells, pericytes, and astrocytes:* For tight junction staining, endothelial
613 cells were fixed with ice cold ethanol for 30 minutes and acetone for 1 minute. For all other staining, ECs,

614 PCs, and ACs were fixed in 4% PFA for 15 min. Fixed monolayers were then washed twice in PBS,
615 blocked for an hour in blocking buffer (5% goat or donkey serum, 0.3% Triton X-100 in PBS), and
616 incubated overnight with appropriate primary antibodies in a diluting solution at 4º C (5% goat or donkey
617 serum; 0.01% Triton X-100 in 1 x PBS). The following day, cells were stained with secondary antibodies
618 in 1 x PBS for 1 hour at room temperature and DAPI (1:5000) for 10 minutes. Imaging was performed on
619 a ZEISS LSM700 confocal microscope using 10x (Plan-Apochromat 10x objective lens) and 20x (Plan
620 Apochromat 20x objective lens).
621
622 *Immunostaining of 3D MIMETAS cultures*: On day 10 post seeding, MIMETAS chips with fixed with
623 either 4% PFA for 15 minutes for standard staining or ethanol/acetone for tight junction visualization. For
624 fixation and blocking, solution was introduced as follows: 100 uL in right channel inlet, 50 uL in right
625 channel outlet, 50 uL in left channel inlet, 50 uL in left channel outlet. Plate was placed on the OrganoFlow
626 for rocking during staining. Chips were blocked for an hour in blocking buffer, and incubated overnight
627 with primary antibodies in diluting solution at 4º C as follows: 25 uL in right channel inlet and outlet; 15
628 uL in left channel inlets and outlets. Cells were washed and incubated with secondary antibodies and
629 DAPI as above. Then, chips were post-fixed with 4% PFA for 15 minutes prior to microscopic imaging.
630
631 **Bulk RNA sequencing, alignment and analysis**:
632 Total RNA was extracted as previously described. RNA samples underwent quality assessment using the
633 Qubit 2.0 Fluorometer, and RNA integrity was assessed using the Agilent TapeStation 4200.
634 Subsequently, RNA sequencing libraries were prepared using the NEBNext Ultra II RNA Library Prep
635 Kit following the manufacturer's protocol. The samples were sequenced in a 2x150bp Paired-End (PE)
636 configuration using the Illumina NovaSeq instrument.
637

638 Previously published samples were obtained from Gene Expression Omnibus (GEO) datasets, including
639 GSE138025, GSE40291, GSE57662, GSE131039, GSE97575, GSE73721, GSE97324, GSE138025,
640 GSE122588, GSE129290, GSE97100, GSE126449, GSE108012, GSE151976, GSE85403, GSE82207,
641 GSE77250, GSE82207, GSE157852, GSE243193, GSE225549, and GSE227501. Quality control for the
642 samples was conducted using FastQC, followed by adapter trimming with Skewer (v0.2.2). The resulting
643 reads were aligned to the human reference genome (hg38) using the STAR aligner, and counts were
644 generated using subread.
645
646 Normalization was performed using the trimmed mean of M-values (TMM) method implemented in the
647 EdgeR R package. Fragments per kilobase of transcript per million mapped reads (FPKM) and Log2
648 counts per million (cpm) matrices were generated to account for library size variations. Differential
649 expression analysis was conducted considering a p-adjusted value < 0.05 and a log2fold change less than
650 -0.25 or greater than 0.25.
651
652 Principal component analysis and Pearson correlation values were computed using the resulting Log_2
653 cpm values. Heatmaps were generated using Min-Max scaling on normalized counts.
654
655
656
657
658

659 **REFERENCES**

660 1 Nance, E., Pun, S. H., Saigal, R. & Sellers, D. L. Drug delivery to the central nervous system.
661 *Nature Reviews Materials* **7**, 314-331 (2022). https://doi.org:10.1038/s41578-021-00394-w
662 2 Eelen, G., de Zeeuw, P., Simons, M. & Carmeliet, P. Endothelial cell metabolism in normal and
663 diseased vasculature. *Circ Res* **116**, 1231-1244 (2015).
664 https://doi.org:10.1161/circresaha.116.302855
665 3 Liebner, S. *et al.* Functional morphology of the blood–brain barrier in health and disease. *Acta*
666 *Neuropathologica* **135**, 311-336 (2018). https://doi.org:10.1007/s00401-018-1815-1
667 4 Marchetti, L. & Engelhardt, B. Immune cell trafficking across the blood-brain barrier in the
668 absence and presence of neuroinflammation. *Vascular Biology* **2**, H1-H18 (2020).
669 https://doi.org:10.1530/vb-19-0033
670 5 Profaci, C. P., Munji, R. N., Pulido, R. S. & Daneman, R. The blood–brain barrier in health and
671 disease: Important unanswered questions. *Journal of Experimental Medicine* **217** (2020).
672 https://doi.org:10.1084/jem.20190062
673 6 Abadier, M. *et al.* Cell surface levels of endothelial ICAM-1 influence the transcellular or
674 paracellular T-cell diapedesis across the blood-brain barrier. *Eur J Immunol* **45**, 1043-1058
675 (2015). https://doi.org:10.1002/eji.201445125
676 7 Trajkovic, M. *et al.* Abnormal thyroid hormone metabolism in mice lacking the
677 monocarboxylate transporter 8. *The Journal of Clinical Investigation* **117**, 627-635 (2007).
678 https://doi.org:10.1172/JCI28253
679 8 Hodge, R. D. *et al.* Conserved cell types with divergent features in human versus mouse cortex.
680 *Nature* **573**, 61-68 (2019). https://doi.org:10.1038/s41586-019-1506-7
681 9 Uchida, Y. *et al.* Comparison of Absolute Protein Abundances of Transporters and Receptors
682 among Blood–Brain Barriers at Different Cerebral Regions and the Blood–Spinal Cord Barrier in
683 Humans and Rats. *Molecular Pharmaceutics* **17**, 2006-2020 (2020).
684 https://doi.org:10.1021/acs.molpharmaceut.0c00178
685 10 Drummond, E. & Wisniewski, T. Alzheimer's disease: experimental models and reality. *Acta*
686 *Neuropathol* **133**, 155-175 (2017). https://doi.org:10.1007/s00401-016-1662-x
687 11 Qosa, H. *et al.* Differences in amyloid-β clearance across mouse and human blood-brain barrier
688 models: kinetic analysis and mechanistic modeling. *Neuropharmacology* **79**, 668-678 (2014).
689 https://doi.org:10.1016/j.neuropharm.2014.01.023
690 12 Xiong, Y., Mahmood, A. & Chopp, M. Animal models of traumatic brain injury. *Nat Rev Neurosci*
691 **14**, 128-142 (2013). https://doi.org:10.1038/nrn3407
692 13 Verscheijden, L. F. M., Koenderink, J. B., de Wildt, S. N. & Russel, F. G. M. Differences in P-
693 glycoprotein activity in human and rodent blood-brain barrier assessed by mechanistic
694 modelling. *Arch Toxicol* **95**, 3015-3029 (2021). https://doi.org:10.1007/s00204-021-03115-y
695 14 Aday, S., Li, W., Karp, J. M. & Joshi, N. An in vitro Blood-brain Barrier Model to Study the
696 Penetration of Nanoparticles. *Bio Protoc* **12**, e4334 (2022).
697 https://doi.org:10.21769/BioProtoc.4334
698 15 Bagchi, S. *et al.* In-vitro blood-brain barrier models for drug screening and permeation studies:
699 an overview. *Drug Des Devel Ther* **13**, 3591-3605 (2019). https://doi.org:10.2147/dddt.S218708
700 16 Linville, R. M. & Searson, P. C. Next-generation in vitro blood–brain barrier models:
701 benchmarking and improving model accuracy. *Fluids and Barriers of the CNS* **18**, 56 (2021).
702 https://doi.org:10.1186/s12987-021-00291-y

17 Schreiner, T. G., Creangă-Murariu, I., Tamba, B. I., Lucanu, N. & Popescu, B. O. In Vitro Modeling of the Blood-Brain Barrier for the Study of Physiological Conditions and Alzheimer's Disease. *Biomolecules* **12** (2022). https://doi.org:10.3390/biom12081136

18 Fujimoto, T. *et al.* Comparison of the rate of dedifferentiation with increasing passages among cell sources for an in vitro model of the blood–brain barrier. *Journal of Neural Transmission* **127**, 1117-1124 (2020). https://doi.org:10.1007/s00702-020-02202-1

19 Helms, H. C. *et al.* In vitro models of the blood–brain barrier: An overview of commonly used brain endothelial cell culture models and guidelines for their use. *Journal of Cerebral Blood Flow & Metabolism* **36**, 862-890 (2016). https://doi.org:10.1177/0271678x16630991

20 Sabbagh, M. F. & Nathans, J. A genome-wide view of the de-differentiation of central nervous system endothelial cells in culture. *Elife* **9** (2020). https://doi.org:10.7554/eLife.51276

21 Faley, S. L. *et al.* iPSC-Derived Brain Endothelium Exhibits Stable, Long-Term Barrier Function in Perfused Hydrogel Scaffolds. *Stem Cell Reports* **12**, 474-487 (2019). https://doi.org:10.1016/j.stemcr.2019.01.009

22 Lippmann, E. S. *et al.* Derivation of blood-brain barrier endothelial cells from human pluripotent stem cells. *Nat Biotechnol* **30**, 783-791 (2012). https://doi.org:10.1038/nbt.2247

23 Qian, T. *et al.* Directed differentiation of human pluripotent stem cells to blood-brain barrier endothelial cells. *Sci Adv* **3**, e1701679 (2017). https://doi.org:10.1126/sciadv.1701679

24 Vatine, G. D. *et al.* Human iPSC-Derived Blood-Brain Barrier Chips Enable Disease Modeling and Personalized Medicine Applications. *Cell Stem Cell* **24**, 995-1005.e1006 (2019). https://doi.org:10.1016/j.stem.2019.05.011

25 Canfield, S. G. *et al.* An isogenic blood-brain barrier model comprising brain endothelial cells, astrocytes, and neurons derived from human induced pluripotent stem cells. *J Neurochem* **140**, 874-888 (2017). https://doi.org:10.1111/jnc.13923

26 Lippmann, E. S., Al-Ahmad, A., Azarin, S. M., Palecek, S. P. & Shusta, E. V. A retinoic acid-enhanced, multicellular human blood-brain barrier model derived from stem cell sources. *Sci Rep* **4**, 4160 (2014). https://doi.org:10.1038/srep04160

27 Stebbins, M. J. *et al.* Differentiation and characterization of human pluripotent stem cell-derived brain microvascular endothelial cells. *Methods* **101**, 93-102 (2016). https://doi.org:10.1016/j.ymeth.2015.10.016

28 Lu, T. M. *et al.* Pluripotent stem cell-derived epithelium misidentified as brain microvascular endothelium requires ETS factors to acquire vascular fate. *Proceedings of the National Academy of Sciences* **118**, e2016950118 (2021). https://doi.org:doi:10.1073/pnas.2016950118

29 Matsuo, K., Engelhardt, B. & Nishihara, H. Differentiation of Human Induced Pluripotent Stem Cells to Brain Microvascular Endothelial Cell-Like Cells with a Mature Immune Phenotype. *JoVE*, e65134 (2023). https://doi.org:doi:10.3791/65134

30 Nishihara, H. *et al.* Advancing human induced pluripotent stem cell-derived blood-brain barrier models for studying immune cell interactions. *Faseb j* **34**, 16693-16715 (2020). https://doi.org:10.1096/fj.202001507RR

31 Hupe, M. *et al.* Gene expression profiles of brain endothelial cells during embryonic development at bulk and single-cell levels. *Science Signaling* **10**, eaag2476 (2017). https://doi.org:doi:10.1126/scisignal.aag2476

32 Sabbagh, M. F. *et al.* Transcriptional and epigenomic landscapes of CNS and non-CNS vascular endothelial cells. *eLife* **7**, e36187 (2018). https://doi.org:10.7554/eLife.36187

747 33 Reyahi, A. *et al.* Foxf2 Is Required for Brain Pericyte Differentiation and Development and
748 Maintenance of the Blood-Brain Barrier. *Developmental Cell* **34**, 19-32 (2015).
749 https://doi.org:https://doi.org/10.1016/j.devcel.2015.05.008
750 34 Cottarelli, A. *et al.* Fgfbp1 promotes blood-brain barrier development by regulating collagen IV
751 deposition and maintaining Wnt/β-catenin signaling. *Development* **147** (2020).
752 https://doi.org:10.1242/dev.185140
753 35 Praca, C. *et al.* Derivation of Brain Capillary-like Endothelial Cells from Human Pluripotent Stem
754 Cell-Derived Endothelial Progenitor Cells. *Stem Cell Reports* **13**, 599-611 (2019).
755 https://doi.org:10.1016/j.stemcr.2019.08.002
756 36 Engelhardt, B. & Liebner, S. Novel insights into the development and maintenance of the
757 blood–brain barrier. *Cell and Tissue Research* **355**, 687-699 (2014).
758 https://doi.org:10.1007/s00441-014-1811-2
759 37 Mikami, Y. *et al.* Chronic airway epithelial hypoxia exacerbates injury in muco-obstructive lung
760 disease through mucus hyperconcentration. *Science Translational Medicine* **15**, eabo7728
761 (2023). https://doi.org:doi:10.1126/scitranslmed.abo7728
762 38 Singh, N. *et al.* Transcriptional profiles of pulmonary artery endothelial cells in pulmonary
763 hypertension. *Sci Rep* **13**, 22534 (2023). https://doi.org:10.1038/s41598-023-48077-6
764 39 Uhl, K. *et al.* Differential Transcriptomic Signatures of Small Airway Cell Cultures Derived from
765 IPF and COVID-19-Induced Exacerbation of Interstitial Lung Disease. *Cells* **12**, 2501 (2023).
766 40 Zhao, Z., Nelson, A. R., Betsholtz, C. & Zlokovic, B. V. Establishment and Dysfunction of the
767 Blood-Brain Barrier. *Cell* **163**, 1064-1078 (2015). https://doi.org:10.1016/j.cell.2015.10.067
768 41 Miller, D. W., Batrakova, E. V., Waltner, T. O., Alakhov, V. & Kabanov, A. V. Interactions of
769 pluronic block copolymers with brain microvessel endothelial cells: evidence of two potential
770 pathways for drug absorption. *Bioconjug Chem* **8**, 649-657 (1997).
771 https://doi.org:10.1021/bc970118d
772 42 Revesz, T. *et al.* Genetics and molecular pathogenesis of sporadic and hereditary cerebral
773 amyloid angiopathies. *Acta Neuropathol* **118**, 115-130 (2009). https://doi.org:10.1007/s00401-
774 009-0501-8
775 43 Santos, C. Y. *et al.* Pathophysiologic relationship between Alzheimer's disease, cerebrovascular
776 disease, and cardiovascular risk: A review and synthesis. *Alzheimers Dement (Amst)* **7**, 69-87
777 (2017). https://doi.org:10.1016/j.dadm.2017.01.005
778 44 Toledo, J. B. *et al.* Contribution of cerebrovascular disease in autopsy confirmed
779 neurodegenerative disease cases in the National Alzheimer's Coordinating Centre. *Brain* **136**,
780 2697-2706 (2013). https://doi.org:10.1093/brain/awt188
781 45 Sweeney, M. D., Sagare, A. P. & Zlokovic, B. V. Blood–brain barrier breakdown in Alzheimer
782 disease and other neurodegenerative disorders. *Nature Reviews Neurology* **14**, 133-150 (2018).
783 https://doi.org:10.1038/nrneurol.2017.188
784 46 Biffi, A. & Greenberg, S. M. Cerebral amyloid angiopathy: a systematic review. *J Clin Neurol* **7**, 1-
785 9 (2011). https://doi.org:10.3988/jcn.2011.7.1.1
786 47 Cottarelli, A. *et al.* Rab7a activation promotes degradation of select tight junction proteins at
787 the blood-brain barrier after ischemic stroke. *bioRxiv* (2023).
788 https://doi.org:10.1101/2023.08.29.555373
789 48 Dimitrijevic, O. B., Stamatovic, S. M., Keep, R. F. & Andjelkovic, A. V. Effects of the chemokine
790 CCL2 on blood-brain barrier permeability during ischemia-reperfusion injury. *J Cereb Blood Flow*
791 *Metab* **26**, 797-810 (2006). https://doi.org:10.1038/sj.jcbfm.9600229

792 49 Schellenberg, A. E. *et al.* Blood-brain barrier disruption in CCL2 transgenic mice during pertussis
793 toxin-induced brain inflammation. *Fluids Barriers CNS* **9**, 10 (2012).
794 https://doi.org:10.1186/2045-8118-9-10
795 50 Guo, F. *et al.* Chemokine CCL2 contributes to BBB disruption via the p38 MAPK signaling
796 pathway following acute intracerebral hemorrhage. *FASEB J* **34**, 1872-1884 (2020).
797 https://doi.org:10.1096/fj.201902203RR
798 51 Shin, Y. J. *et al.* Amyloid beta peptides (Abeta) from Alzheimer's disease neuronal secretome
799 induce endothelial activation in a human cerebral microvessel model. *Neurobiol Dis* **181**,
800 106125 (2023). https://doi.org:10.1016/j.nbd.2023.106125
801 52 Kano, A. *et al.* Endothelial cells require STAT3 for protection against endotoxin-induced
802 inflammation. *J Exp Med* **198**, 1517-1525 (2003). https://doi.org:10.1084/jem.20030077
803 53 Mehla, J. *et al.* STAT3 inhibitor mitigates cerebral amyloid angiopathy and parenchymal amyloid
804 plaques while improving cognitive functions and brain networks. *Acta Neuropathol Commun* **9**,
805 193 (2021). https://doi.org:10.1186/s40478-021-01293-5
806 54 Faal, T. *et al.* Induction of Mesoderm and Neural Crest-Derived Pericytes from Human
807 Pluripotent Stem Cells to Study Blood-Brain Barrier Interactions. *Stem Cell Reports* **12**, 451-460
808 (2019). https://doi.org:https://doi.org/10.1016/j.stemcr.2019.01.005
809 55 Stebbins, M. J. *et al.* Human pluripotent stem cell-derived brain pericyte-like cells induce blood-
810 brain barrier properties. *Sci Adv* **5**, eaau7375 (2019). https://doi.org:10.1126/sciadv.aau7375
811 56 Tcw, J. *et al.* An Efficient Platform for Astrocyte Differentiation from Human Induced
812 Pluripotent Stem Cells. *Stem Cell Reports* **9**, 600-614 (2017).
813 https://doi.org:https://doi.org/10.1016/j.stemcr.2017.06.018
814 57 Ehlers, H. *et al.* Vascular inflammation on a chip: A scalable platform for trans-endothelial
815 electrical resistance and immune cell migration. *Front Immunol* **14**, 1118624 (2023).
816 https://doi.org:10.3389/fimmu.2023.1118624
817 58 Wevers, N. R. *et al.* A perfused human blood-brain barrier on-a-chip for high-throughput
818 assessment of barrier function and antibody transport. *Fluids Barriers CNS* **15**, 23 (2018).
819 https://doi.org:10.1186/s12987-018-0108-3
820 59 Patsch, C. *et al.* Generation of vascular endothelial and smooth muscle cells from human
821 pluripotent stem cells. *Nat Cell Biol* **17**, 994-1003 (2015). https://doi.org:10.1038/ncb3205
822 60 Lim, R. G. *et al.* Huntington's Disease iPSC-Derived Brain Microvascular Endothelial Cells Reveal
823 WNT-Mediated Angiogenic and Blood-Brain Barrier Deficits. *Cell Rep* **19**, 1365-1377 (2017).
824 https://doi.org:10.1016/j.celrep.2017.04.021
825 61 Blanchard, J. W. *et al.* Reconstruction of the human blood-brain barrier in vitro reveals a
826 pathogenic mechanism of APOE4 in pericytes. *Nat Med* **26**, 952-963 (2020).
827 https://doi.org:10.1038/s41591-020-0886-4
828 62 Stanton, A. E. *et al.* Engineered 3D Immuno-Glial-Neurovascular Human miBrain Model. *bioRxiv*,
829 2023.2008.2015.553453 (2024). https://doi.org:10.1101/2023.08.15.553453
830 63 Jamieson, J. J., Linville, R. M., Ding, Y. Y., Gerecht, S. & Searson, P. C. Role of iPSC-derived
831 pericytes on barrier function of iPSC-derived brain microvascular endothelial cells in 2D and 3D.
832 *Fluids and Barriers of the CNS* **16**, 15 (2019). https://doi.org:10.1186/s12987-019-0136-7
833 64 Linville, R. M. *et al.* Long-Term Cryopreservation Preserves Blood-Brain Barrier Phenotype of
834 iPSC-Derived Brain Microvascular Endothelial Cells and Three-Dimensional Microvessels. *Mol*
835 *Pharm* **17**, 3425-3434 (2020). https://doi.org:10.1021/acs.molpharmaceut.0c00484

65 Roudnicky, F. *et al.* Identification of a combination of transcription factors that synergistically increases endothelial cell barrier resistance. *Scientific Reports* **10**, 3886 (2020). https://doi.org:10.1038/s41598-020-60688-x

66 Lian, X. *et al.* Efficient differentiation of human pluripotent stem cells to endothelial progenitors via small-molecule activation of WNT signaling. *Stem Cell Reports* **3**, 804-816 (2014). https://doi.org:10.1016/j.stemcr.2014.09.005

67 Porkolab, G. *et al.* Synergistic induction of blood-brain barrier properties. *Proc Natl Acad Sci U S A* **121**, e2316006121 (2024). https://doi.org:10.1073/pnas.2316006121

68 Parodi-Rullán, R., Ghiso, J., Cabrera, E., Rostagno, A. & Fossati, S. Alzheimer's amyloid β heterogeneous species differentially affect brain endothelial cell viability, blood-brain barrier integrity, and angiogenesis. *Aging Cell* **19**, e13258 (2020). https://doi.org:https://doi.org/10.1111/acel.13258

69 Moir, R. D., Lathe, R. & Tanzi, R. E. The antimicrobial protection hypothesis of Alzheimer's disease. *Alzheimers Dement* **14**, 1602-1614 (2018). https://doi.org:10.1016/j.jalz.2018.06.3040

70 Yu, J. *et al.* Induced pluripotent stem cell lines derived from human somatic cells. *Science* **318**, 1917-1920 (2007). https://doi.org:10.1126/science.1151526

71 Tchieu, J. *et al.* NFIA is a gliogenic switch enabling rapid derivation of functional human astrocytes from pluripotent stem cells. *Nat Biotechnol* **37**, 267-275 (2019). https://doi.org:10.1038/s41587-019-0035-0

72 Maherali, N. *et al.* A high-efficiency system for the generation and study of human induced pluripotent stem cells. *Cell Stem Cell* **3**, 340-345 (2008). https://doi.org:10.1016/j.stem.2008.08.003

73 Reya, T. *et al.* A role for Wnt signalling in self-renewal of haematopoietic stem cells. *Nature* **423**, 409-414 (2003). https://doi.org:10.1038/nature01593

74 Song, S. *et al.* Efficient Derivation of Excitatory and Inhibitory Neurons from Human Pluripotent Stem Cells Stably Expressing Direct Reprogramming Factors. *Curr Protoc* **1**, e141 (2021). https://doi.org:10.1002/cpz1.141

75 Fu, B. M., Zhao, Z. & Zhu, D. Blood-Brain Barrier (BBB) Permeability and Transport Measurement In Vitro and In Vivo. *Methods Mol Biol* **2367**, 105-122 (2021). https://doi.org:10.1007/7651_2020_308

76 Suarez-Arnedo, A. *et al.* An image J plugin for the high throughput image analysis of in vitro scratch wound healing assays. *PLoS One* **15**, e0232565 (2020). https://doi.org:10.1371/journal.pone.0232565

77 Bankhead, P. *et al.* QuPath: Open source software for digital pathology image analysis. *Scientific Reports* **7**, 16878 (2017). https://doi.org:10.1038/s41598-017-17204-5

78 Stine, W. B., Jr., Dahlgren, K. N., Krafft, G. A. & LaDu, M. J. In vitro characterization of conditions for amyloid-beta peptide oligomerization and fibrillogenesis. *J Biol Chem* **278**, 11612-11622 (2003). https://doi.org:10.1074/jbc.M210207200

79 Kim, Y. A. *et al.* RNA methyltransferase NSun2 deficiency promotes neurodegeneration through epitranscriptomic regulation of tau phosphorylation. *Acta Neuropathol* **145**, 29-48 (2023). https://doi.org:10.1007/s00401-022-02511-7

880 **FIGURE LEGENDS**

881 **Figure 1. rBMECs generated through FOXF2/ZIC3 transcriptional reprogramming express key**
882 **EC markers and respond to angiogenic stimuli. A)** Schematic diagram for the generation of BBB
883 primed ECs (bpECs) and reprogrammed BMECs (rBMECs) from human induced pluripotent stem cells
884 (hiPSCs). **B)** Representative flow cytometry plots showing the fraction of $CD31^+$/VE-$CADHERIN^+$ ECs
885 isolated after 10 days of the initial differentiation (sort A; bpECs) and 14 days after FOXF2/ZIC3
886 transduction (sort B; rBMECs). **C)** Dotted bar graph of the fraction of $CD31^+$/VE-$CADHERIN^+$ bpECs
887 and rBMECs at 14 days post FOXF2/ZIC3 transduction; n = 5, unpaired t-test, **p<0.01. **D-F)**
888 Representative immunofluorescence staining of HBMECs, bpECs and rBMECs for EC (CD31, VE-
889 CADHERIN) and TJ (OCCLUDIN, CLAUDIN-5, ZO-1) proteins. DAPI (blue in merged images) labels
890 the nuclei. Scale bar = 25 μm. **G-H)** Representative western blots and quantification for CLAUDIN-5 and
891 OCCLUDIN expression. Mean ± SD, n = 9 from three experiments, unpaired t-test, **p<0.1, ***p<0.001.
892 **I)** Proliferative index quantification after cell migration assay; n = 8-9 from three experiments, one-way
893 ANOVA, ****p<0.0001. **J)** Quantification of the normalized area (pixels) of the wound region in the
894 scratch assay; repeated measures ANOVA with Bonferroni correction; n = 9 from three experiments,
895 *p<0.05, **p<0.1, ***p<0.001, ****p<0.0001. **K)** Quantification of angiogenic potential; n = 9 from
896 three experiments, one-way ANOVA, ns p>0.05, ***p<0.001. (See also **Figure S1**).

897

898 **Figure 2. The rBMEC transcriptome shows higher expression of BBB molecular identity genes**
899 **compared to primary HBMECs. A)** PCA plot illustrating endothelial vs. epithelial identity of 155
900 sequenced RNA samples from several published studies and this study. **B)** PCA plot illustrating peripheral
901 vs. brain EC identity of 58 differentiated and primary EC samples from published studies and this study.
902 **C)** Volcano plot highlighting significantly up- and downregulated BBB-specific genes in rBMECs
903 compared to HBMECs. **D**) Upregulated GO analysis pathways in rBMECs compared to HBMECs. **E-**
904 **H)** Heatmap of BBB-specific genes (TJ proteins, Transporters, Bulk and Receptor-Mediated Transcytosis,

905 Extracellular Matrix, and CNS EC genes) between rBMEC and HBMECs. The upregulated genes in
906 rBMECs are shown in red and the upregulated genes in HBMECs are shown in blue.
907
908 **Figure 3. rBMECs have strong functional BBB properties and respond to inflammatory stimuli. A-**
909 **B)** Representative ECIS TEER recording and dotted bar graph of the area under the curve (AUC)
910 quantification for IMR90 hiPSC-derived bpECs, rBMECs, and primary HBMECs. The red box indicates
911 the period used for the AUC quantification. Mean ± SD, n = 6-8 from 3-4 experiments, one-way ANOVA,
912 **p<0.01. **C-D)** Dotted bar graphs of the transwell permeability across EC monolayers to sodium
913 fluorescein (NaF) and 3kDa dextran. Mean ± SD, n = 9 from three experiments, ANOVA with Kruskal-
914 Wallis Test, *p<0.05, **p<0.01, ***p<0.001. **E-F)** Representative histograms and quantification of BSA-
915 AF594 uptake in HBMECs, bpECs and rBMECs. Mean ± SD, n = 9 from three experiments, one-way
916 ANOVA, ****p<0.0001. **G-I)** Representative histograms of Rhodamine123 MFI and PGP efflux in
917 HBMECs, bpECs and rBMECs. n = 9 from 3 independent experiments, one-way ANOVA, **p<0.01. **J-**
918 **K)** Representative ECIS TEER and dotted bar graph of the AUC quantification for rBMECs during 72 hr
919 treatment with F12 vehicle or 1 uM oAβ42 (red box), n = 9-10 from three experiments, unpaired t-test, ns
920 p>0.05. **L)** RT-qPCR for several inflammatory genes in rBMECs after 6 hours of 500nM oAβ42
921 treatment; n = 8-9 from three experiments, unpaired t-test, **p<0.01, ***p<0.001, ****p<0.0001. **M)**
922 VCAM-1 and ICAM-1 surface expression quantification after 6 hours 500nM oAβ42; n = 6 from two
923 experiments, unpaired t-test, **<0.01, ****<0.0001. **N-O)** Representative western blots and
924 quantification for VCAM-1 and ICAM-1 after 6 hours of 500nM oAβ42; n = 6 from two experiments,
925 unpaired t-test, ***<0.001.
926
927 **Figure 4: rBMECs tubules have improved barrier properties when co-cultured with iPSC-derived**
928 **astrocytes and pericytes in a 3D microfluidic NVU system. A)** Schematic diagram for generating the
929 3D NVU/BBB microfluidic system. **B)** Brightfield images of EC tubules formed by HBMECs and

930 rBMECs with (right) and without (left) primary or iPSC-derived astrocytes and pericytes, respectively.
931 **C)** Representative IF staining of rBMEC tubules for CD31 and VE-CADHERIN (top) or ZO-1 and
932 CLAUDIN-5 (bottom). Scale bar = 50 µm **D)** 3D image of IF staining within the 3D NVU microfluidics
933 system showing iPCs (PDGFRβ) and iACs (S100β) migrating from the "brain" to the "blood" channel
934 where the rBMECs tubules are located. **E)** Representative triculture staining with rBMECs (ZO-1), iACs
935 (S100β), and iPCs (PDGFRβ) in the blood channel; cross sectional view shows tubule with a lumen. **F)**
936 Representative image showing diffusion of fluorescent tracers through leaky and tight tubules. **G-H)** Box
937 plots showing the normalized intensity of 70 kDa dextran and biocytin (890 Da) tracers in the middle
938 channel indicative of permeability; n = 36-41 NVU chips from three experiments. two-way ANOVA,
939 **$p<0.01$, ****$p<0.0001$. **I)** Dotted bar graph of the TEER measurement in the 3D NVU/BBB
940 microphysiological system using the OrganoTEER for EC tubules alone or together with PCs/ACs; n =
941 30-48 chips over three experiments, one-way ANOVA, ****$p<0.0001$, *$p<0.05$.

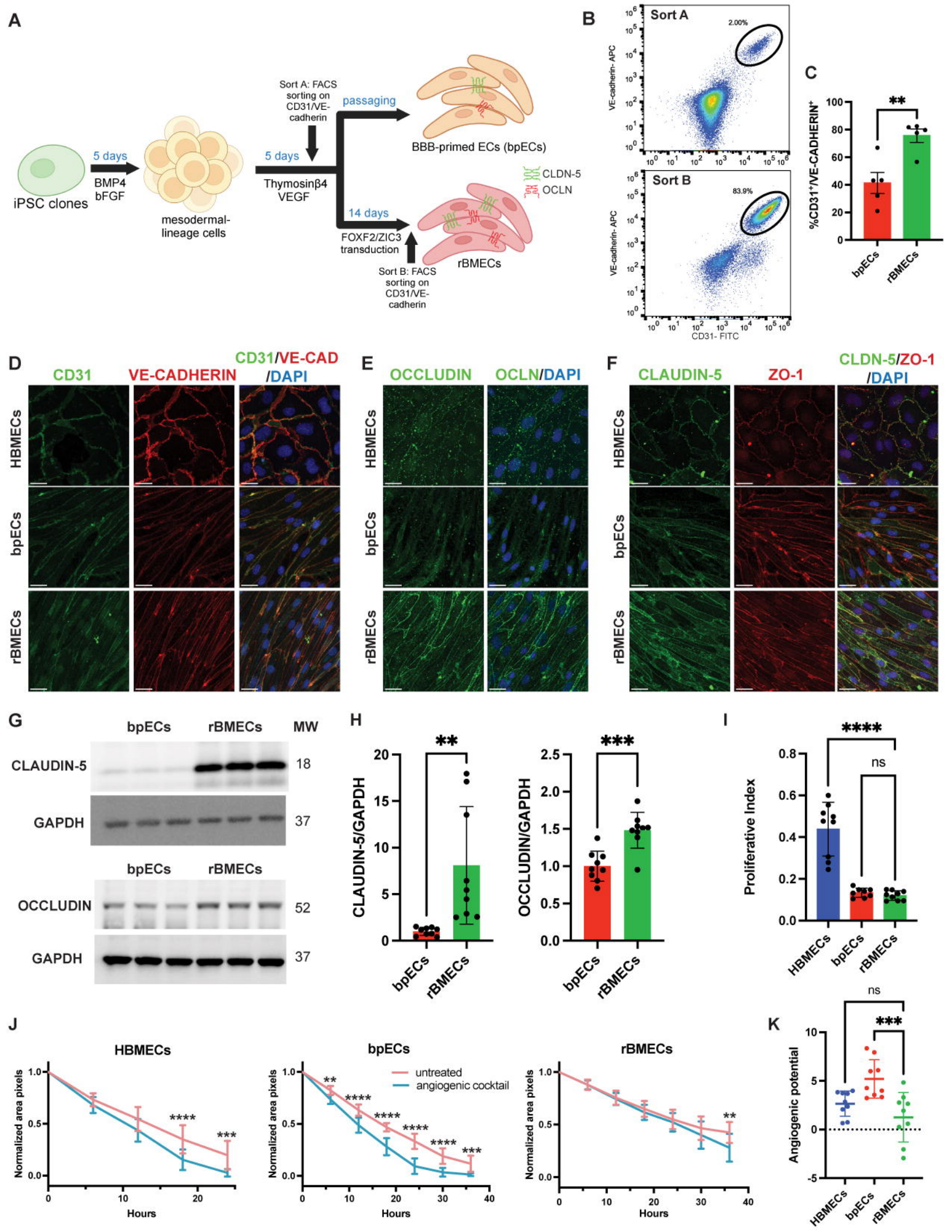
A
iPSC clones
5 days
BMP4
bFGF
mesodermal-lineage cells
Sort A: FACS sorting on CD31/VE-cadherin
5 days
Thymosinβ4
VEGF
passaging
BBB-primed ECs (bpECs)
14 days
FOXF2/ZIC3 transduction
Sort B: FACS sorting on CD31/VE-cadherin
rBMECs
CLDN-5
OCLN
B
Sort A
2.00%
Sort B
83.9%
VE-cadherin- APC
CD31- FITC
C
%CD31+/VE-CADHERIN+
bpECs
rBMECs
D
CD31
VE-CADHERIN
CD31/VE-CAD /DAPI
HBMECs
bpECs
rBMECs
E
OCCLUDIN
OCLN/DAPI
F
CLAUDIN-5
ZO-1
CLDN-5/ZO-1 /DAPI
G
bpECs
rBMECs
MW
CLAUDIN-5
18
GAPDH
37
OCCLUDIN
52
H
CLAUDIN-5/GAPDH
OCCLUDIN/GAPDH
I
Proliferative Index
ns
HBMECs
J
HBMECs
bpECs
rBMECs
untreated
angiogenic cocktail
Normalized area pixels
Hours
K
Angiogenic potential

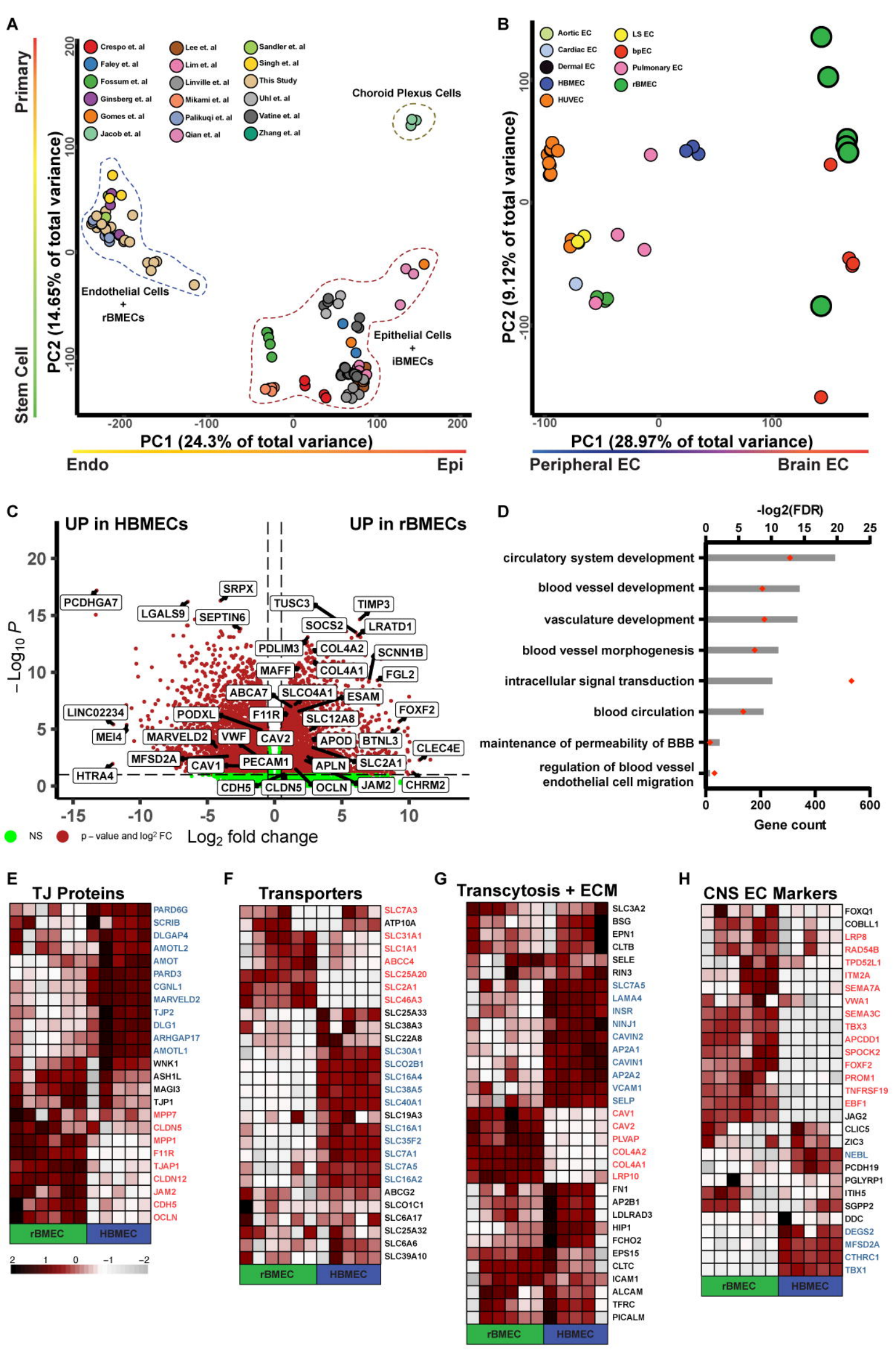
A
Primary
Stem Cell
Crespo et. al
Faley et. al
Fossum et. al
Ginsberg et. al
Gomes et. al
Jacob et. al
Lee et. al
Lim et. al
Linville et. al
Mikami et. al
Palikuqi et. al
Qian et. al
Sandler et. al
Singh et. al
This Study
Uhl et. al
Vatine et. al
Zhang et. al
Choroid Plexus Cells
Endothelial Cells
+
rBMECs
Epithelial Cells
+
iBMECs
PC2 (14.65% of total variance)
PC1 (24.3% of total variance)
Endo
Epi
B
Aortic EC
Cardiac EC
Dermal EC
HBMEC
HUVEC
LS EC
bpEC
Pulmonary EC
rBMEC
PC2 (9.12% of total variance)
PC1 (28.97% of total variance)
Peripheral EC
Brain EC
C
UP in HBMECs
UP in rBMECs
PCDHGA7
LGALS9
SEPTIN6
SRPX
TUSC3
TIMP3
SOCS2
LRATD1
PDLIM3
COL4A2
SCNN1B
MAFF
COL4A1
FGL2
ABCA7
SLCO4A1
ESAM
LINC02234
PODXL
F11R
SLC12A8
FOXF2
MEI4
MARVELD2
VWF
CAV2
APOD
BTNL3
CLEC4E
MFSD2A
CAV1
PECAM1
APLN
SLC2A1
HTRA4
CDH5
CLDN5
OCLN
JAM2
CHRM2
– Log10 P
Log2 fold change
NS
p – value and log2 FC
D
-log2(FDR)
circulatory system development
blood vessel development
vasculature development
blood vessel morphogenesis
intracellular signal transduction
blood circulation
maintenance of permeability of BBB
regulation of blood vessel endothelial cell migration
Gene count
E
TJ Proteins
PARD6G
SCRIB
DLGAP4
AMOTL2
AMOT
PARD3
CGNL1
MARVELD2
TJP2
DLG1
ARHGAP17
AMOTL1
WNK1
ASH1L
MAGI3
TJP1
MPP7
CLDN5
MPP1
F11R
TJAP1
CLDN12
JAM2
CDH5
OCLN
rBMEC
HBMEC
F
Transporters
SLC7A3
ATP10A
SLC31A1
SLC1A1
ABCC4
SLC25A20
SLC2A1
SLC46A3
SLC25A33
SLC38A3
SLC22A8
SLC30A1
SLCO2B1
SLC16A4
SLC38A5
SLC40A1
SLC19A3
SLC16A1
SLC35F2
SLC7A1
SLC7A5
SLC16A2
ABCG2
SLCO1C1
SLC6A17
SLC25A32
SLC6A6
SLC39A10
rBMEC
HBMEC
G
Transcytosis + ECM
SLC3A2
BSG
EPN1
CLTB
SELE
RIN3
SLC7A5
LAMA4
INSR
NINJ1
CAVIN2
AP2A1
CAVIN1
AP2A2
VCAM1
SELP
CAV1
CAV2
PLVAP
COL4A2
COL4A1
LRP10
FN1
AP2B1
LDLRAD3
HIP1
FCHO2
EPS15
CLTC
ICAM1
ALCAM
TFRC
PICALM
rBMEC
HBMEC
H
CNS EC Markers
FOXQ1
COBLL1
LRP8
RAD54B
TPD52L1
ITM2A
SEMA7A
VWA1
SEMA3C
TBX3
APCDD1
SPOCK2
FOXF2
PROM1
TNFRSF19
EBF1
JAG2
CLIC5
ZIC3
NEBL
PCDH19
PGLYRP1
ITIH5
SGPP2
DDC
DEGS2
MFSD2A
CTHRC1
TBX1
rBMEC
HBMEC

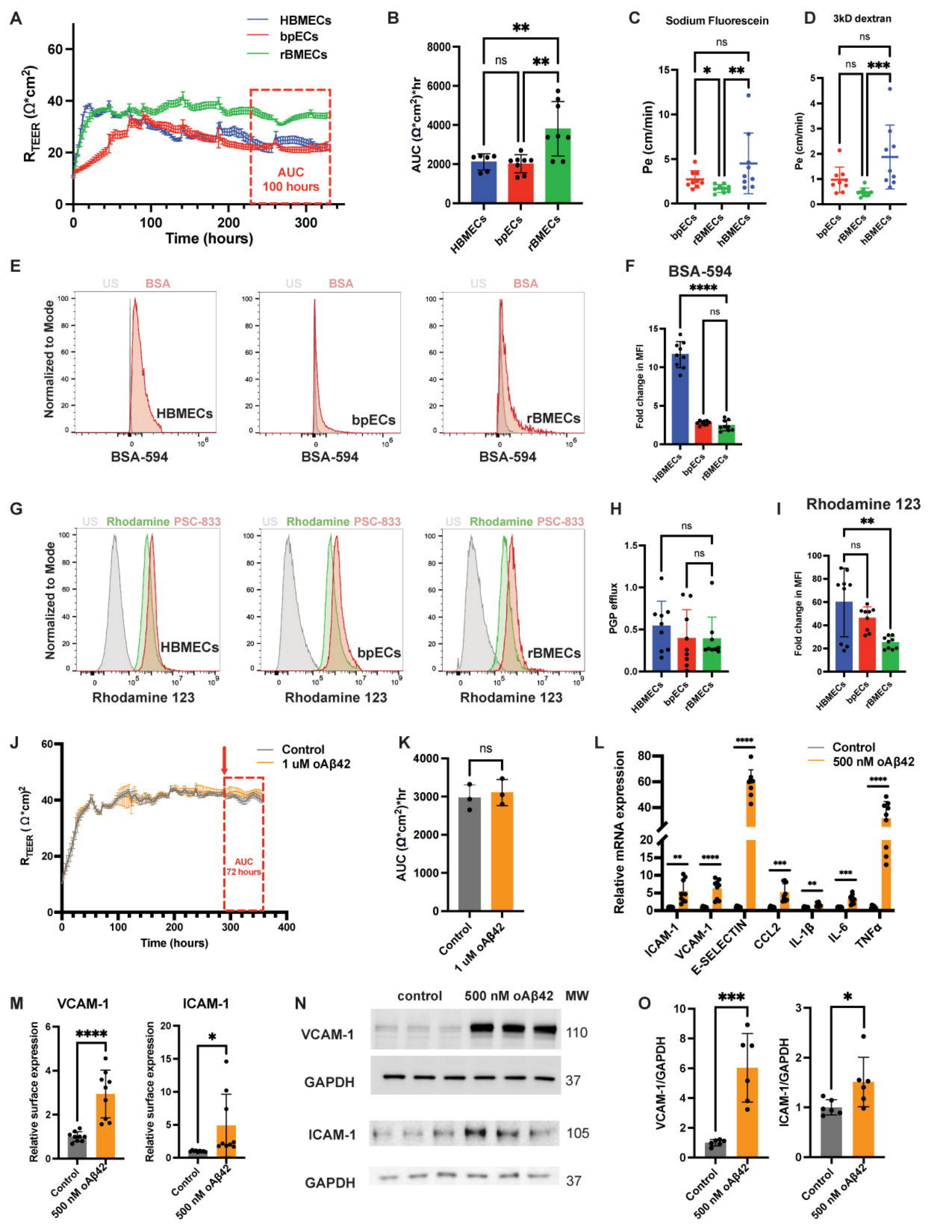
A
HBMECs
bpECs
rBMECs
R_{TEER} (Ω*cm^2)
Time (hours)
AUC
100 hours
B
AUC (Ω*cm^2)*hr
ns
**
**
HBMECs
bpECs
rBMECs
C
Sodium Fluorescein
Pe (cm/min)
ns
*
**
bpECs
rBMECs
hBMECs
D
3kD dextran
Pe (cm/min)
ns
ns
***
bpECs
rBMECs
hBMECs
E
US
BSA
Normalized to Mode
HBMECs
bpECs
rBMECs
BSA-594
F
BSA-594
Fold change in MFI
****
ns
HBMECs
bpECs
rBMECs
G
US
Rhodamine
PSC-833
Normalized to Mode
HBMECs
bpECs
rBMECs
Rhodamine 123
H
PGP efflux
ns
ns
HBMECs
bpECs
rBMECs
I
Rhodamine 123
Fold change in MFI
**
ns
HBMECs
bpECs
rBMECs
J
Control
1 uM oAβ42
R_{TEER} (Ω*cm)^2
AUC
72 hours
Time (hours)
K
AUC (Ω*cm^2)*hr
ns
Control
1 uM oAβ42
L
Control
500 nM oAβ42
Relative mRNA expression
ICAM-1
VCAM-1
E-SELECTIN
CCL2
IL-1β
IL-6
TNFα
M
VCAM-1
ICAM-1
Relative surface expression
****
*
Control
500 nM oAβ42
N
control
500 nM oAβ42
MW
VCAM-1
110
GAPDH
37
ICAM-1
105
GAPDH
37
O
VCAM-1/GAPDH
ICAM-1/GAPDH
***
*
Control
500 nM oAβ42

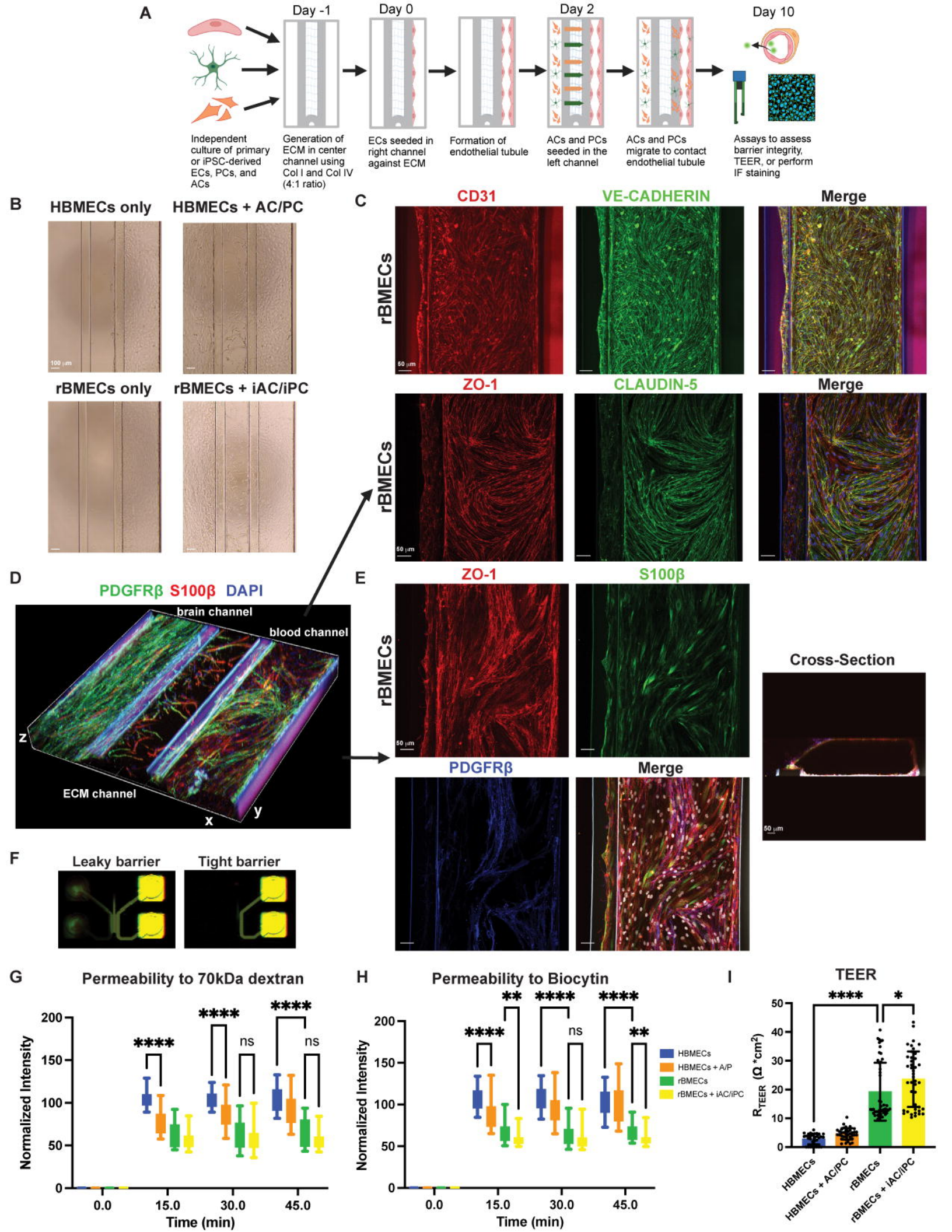
A
Day -1
Day 0
Day 2
Day 10
Independent culture of primary or iPSC-derived ECs, PCs, and ACs
Generation of ECM in center channel using Col I and Col IV (4:1 ratio)
ECs seeded in right channel against ECM
Formation of endothelial tubule
ACs and PCs seeded in the left channel
ACs and PCs migrate to contact endothelial tubule
Assays to assess barrier integrity, TEER, or perform IF staining
B
HBMECs only
HBMECs + AC/PC
rBMECs only
rBMECs + iAC/iPC
100 µm
C
CD31
VE-CADHERIN
Merge
rBMECs
ZO-1
CLAUDIN-5
Merge
rBMECs
50 µm
D
PDGFRβ S100β DAPI
brain channel
blood channel
ECM channel
z
x
y
E
ZO-1
S100β
rBMECs
PDGFRβ
Merge
Cross-Section
50 µm
F
Leaky barrier
Tight barrier
G
Permeability to 70kDa dextran
Normalized Intensity
Time (min)
0.0
15.0
30.0
45.0
****
ns
H
Permeability to Biocytin
Normalized Intensity
Time (min)
HBMECs
HBMECs + A/P
rBMECs
rBMECs + iAC/iPC
I
TEER
R_{TEER} (Ω *cm^2)
HBMECs
HBMECs + AC/PC
rBMECs
rBMECs + iAC/iPC